HHS Public Access

Author manuscript

Immunity. Author manuscript; available in PMC 2024 April 11.

Published in final edited form as:

Immunity. 2023 April 11; 56(4): 847–863.e8. doi:10.1016/j.immuni.2023.03.001.

A transcriptionally distinct subset of Influenza-specific effector memory B cells predicts long-lived antibody responses to vaccination in humans

Anoma Nellore[1,*], **Esther Zumaquero**[2], **Christopher D. Scharer**[3], **Christopher F. Fucile**[4], **Christopher M. Tipton**[5], **R. Glenn King**[2], **Tian Mi**[3], **Betty Mousseau**[2], **John E. Bradley**[6], **Fen Zhou**[2], **Stuti Mutneja**[1], **Paul A. Goepfert**[1], **Jeremy M. Boss**[3], **Troy D. Randall**[6], **Ignacio Sanz**[5], **Alexander F. Rosenberg**[2,4], **Frances E. Lund, PhD**[2,*]

[1]Dept. of Medicine, Division of Infectious Disease at The University of Alabama at Birmingham, Birmingham, AL 35294 USA

[2]Dept of Microbiology at The University of Alabama at Birmingham, Birmingham, AL 35294 USA

[3]Dept. of Microbiology and Immunology, Emory University School of Medicine, Atlanta, GA 30322, USA

[4]Informatics Institute at The University of Alabama at Birmingham, Birmingham, AL 35294 USA

[5]Department of Medicine, Division of Rheumatology, Emory University School of Medicine, Atlanta, GA 30322, USA

[6]Dept. of Medicine, Division of Clinical Immunology and Rheumatology at The University of Alabama at Birmingham, Birmingham, AL 35294 USA

Summary

Seasonal influenza vaccination elicits hemagglutinin (HA)-specific memory B (Bmem) cells, and although multiple Bmem cell populations have been characterized, considerable heterogeneity exists. We found that HA-specific human Bmem cells differed in expression of surface marker FcRL5 and transcriptional factor T-bet. FcRL5^{+}T-bet^{+} Bmem cells were transcriptionally similar to effector-like memory cells while T-bet^{neg}FcRL5^{neg} Bmem cells exhibited stem-like central

[*]Co-corresponding authors: flund@uab.edu, anellore@uabmc.edu.
Lead Contact: Frances E. Lund, PhD, Dept of Microbiology, University of Alabama at Birmingham, 276 BBRB Box 11, 1720 2nd Avenue South, Birmingham AL 35294-2170, flund@uab.edu

Author Contributions: F.E.L. conceived the idea for the project and secured the initial funding. F.E.L. and A.N. designed the experiments that were performed by A.N., E.Z., C.D.S., R.G.K, C.M.T., B.M. and F.Z. B cell tetramers were developed and produced by J.E.B. Human samples used in this study were obtained via the Alabama Vaccine Research Clinic, directed by P.A.G. Bioinformatic analyses were performed by A.F.R, C.D.S., C.F. and T.M. All other data was analyzed by A.N and F.E.L. A.N., A.F.R. and F.E.L wrote the manuscript and prepared final figures. Critical feedback on the project and manuscript were provided by A.F.R, T.D.R, J.F.K., I.S., and J.M.B.

Declarations of Interest
The authors declare no competing interests.

Inclusion and Diversity
We support inclusive, diverse, and equitable conduct of research.

memory properties. FcRL5$^+$ Bmem cells did not express plasma cell-commitment factors but did express transcriptional, epigenetic, metabolic and functional programs that poised these cells for antibody production. Accordingly, HA$^+$ T-bet$^+$ Bmem cells at day 7 post-vaccination expressed intracellular immunoglobulin, and tonsil-derived FcRL5$^+$ Bmem cells differentiated more rapidly into antibody-secreting cells (ASCs) *in vitro*. The T-bet$^+$ Bmem cell response positively correlated with long-lived humoral immunity, and clonotypes from T-bet$^+$ Bmem cells were represented in the secondary ASC response to repeat vaccination, suggesting that this effector-like population predicts influenza vaccine durability and recall potential.

Graphical Abstract

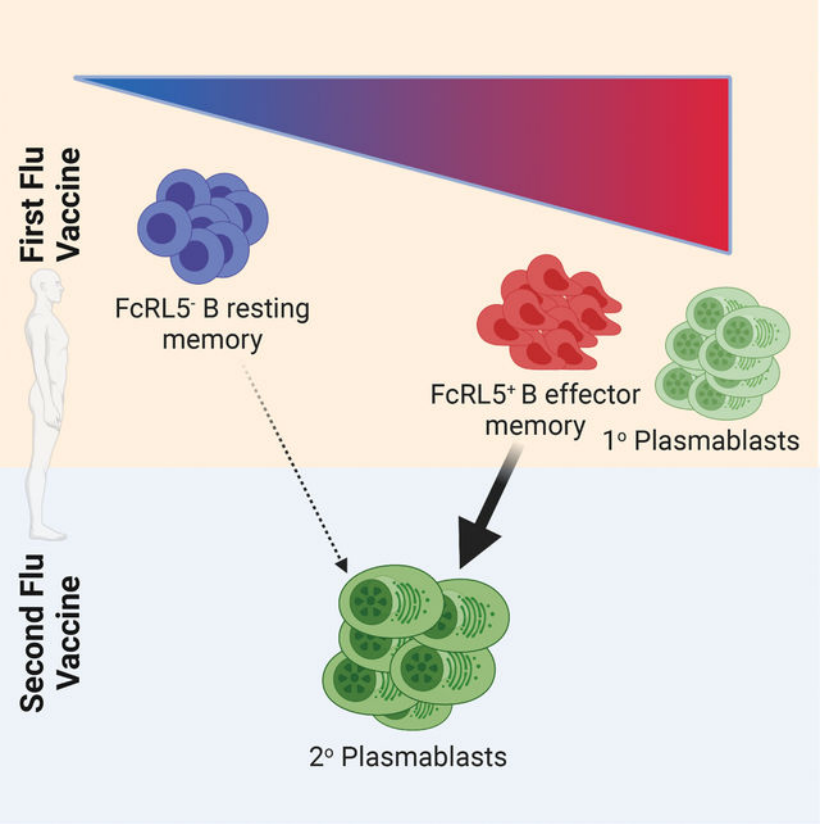

eTOC

Seasonal influenza vaccination recalls pre-existing memory B cells for immune protection. Here Nellore et. al. show that intramuscular influenza vaccination elicits a population of effector memory B cells that are transcriptionally, epigenetically and metabolically poised for antibody production. The magnitude of this FcRL5- and T-bet-expressing effector memory subset response correlates with long-lived antibody responses to influenza vaccination.

Keywords

T-bet; memory B cells; plasmablasts; influenza vaccination; durable immunity

Introduction

Following exposure to previously encountered antigens (Ag), the immune system initiates a recall response dominated by pre-existing memory B (Bmem) cells[1] that can either enter the GC[2] to produce new daughter cells or can rapidly proliferate and differentiate into short-lived plasmablasts (PB), which produce antibodies (Ab) that decrease morbidity and mortality[3]. The cues that direct some Bmem cells toward this early protective "effector-like" fate and the relationship between effector Bmem cells and other GC-derived or extrafollicular Bmem cell populations are not well understood[4].

Prior studies of the $CD8^+$ T cell memory demonstrate that transcription factors (TF) like BACH2 and TCF7 are critical for maintenance of the stem-like properties of memory T cells[5,6], while TFs like BATF and T-bet confer memory T cells with rapid effector potential[7,8]. Many of these same fate-guiding TFs are also expressed by different B cell subsets. For example, BACH2 maintains Bmem cell identity[9] and must be repressed[10,11] during Bmem cell differentiation into antibody secreting cells (ASCs) while T-bet is reported to support ASC formation by mouse Bmem cells responding to flu infection[12]. Although circulating T-bet expressing HA-specific Bmem cells have been observed in flu-vaccinated individuals[13,14], this subset has not been examined in detail because the markers typically used to subdivide Bmem cells, like CD27 and CD21, do not resolve the $CD27^+$ Bmem cell compartment into discrete T-bet-expressing and $T\text{-}bet^{neg}$ populations.

To address how T-bet expressing human Bmem cells contribute to vaccine responses, we used FcRL5 as a cell surface surrogate marker to subdivide the inactivated influenza vaccine (IIV)-elicited human hemagglutinin (HA)-specific Bmem cell compartment into T-bet expressing and non-expressing subpopulations. Here, we show that $FcRL5^+$ and $FcRL5^{neg}$ subsets are clonally, transcriptionally, epigenetically, and functionally distinct from one another. The $T\text{-}bet^+$ $FcRL5^+$ response to IIV correlates with durable vaccine-induced humoral immunity and can be recalled one year later, indicating that these "effector-like" Bmem cells not only contribute to humoral immunity but may also represent an easily measured early biomarker for IIV durability.

Results

Influenza-specific $FcRL5^+T\text{-}bet^+$ Bmem cells represent a phenotypic and clonally distinct subset.

A study[12] using mouse B cells suggests that Bmem cells with effector potential express T-bet. To evaluate whether T-bet expressing human Bmem cells exhibit effector attributes, we used fluorochrome-conjugated H1 and H3 HA tetramers to characterize circulating HA-specific (HA^+) B cells in healthy donors (HD) immunized with seasonal IIV. By day 7 (D7) post-IIV we detected ASCs/PBs (Fig. S1A–B) and IgD^{neg} H1-specific B cells (Fig. 1A). These B cells could be subdivided into a population co-expressing T-bet and Fc receptor like 5 (FcRL5) and a $T\text{-}bet^{neg}FcRL5^{neg}$ population (Fig. 1B). To address whether the $T\text{-}bet^+FcRL5^+$ subset was phenotypically related to other flu-specific Bmem cell subsets, we examined expression of T-bet within the previously described $CD71^+$ Bmem cell subset[15] and the $CD21^{lo}$ subsets[13,14]. Consistent with prior studies of D14 IIV-elicited B cells[14] (Fig.

S1C), we observed that the D7 HA-specific CD21^{lo} Bmem cell subset contained both T-bet^{+} and T-bet^{neg} cells (Fig. S1D) and that T-bet^{+} and T-bet^{neg} cells were both found within the D7 HA-specific CD71^{+} Bmem cell subset[15] (Fig. S1E). Subdividing the IgD^{neg} HA^{+} B cells using T-bet or FcRL5 expression, revealed that most of the HA-specific B cells on D7 post-IIV expressed the canonical memory marker CD27 (Fig. 1C). However, T-bet^{neg} and T-bet^{+} HA^{+} B cells could be distinguished by expression of CXCR5, CCR7 and CD62L, which were higher in T-bet^{neg} cells, and CXCR3, which was increased in the T-bet^{+} cells (Fig. 1C). Comparison of the immunoglobulin (Ig) isotype and somatic mutation frequencies in the heavy chain variable region (V_H) of the BCRs (Table S1) expressed by FcRL5^{+} and FcRL5^{neg} IgD^{neg} H3-specific B cell populations indicated that isotype-switched B cells predominated in both subsets (Fig. 1D, Table S1) and that both populations exhibited similar frequencies of V_H mutations (Fig. 1E, Fig. S1F–G), even when the analysis was restricted to isotype-switched B cells (Fig. S1H–J). Both populations could still be detected at D120 post-vaccination (Fig. S1K–M) and a comparison of BCR clonotypes in the circulating D7 HA-specific FcRL5^{+} and FcRL5^{neg} subsets with the BCR clonotypes found in D120 circulating IgD^{neg} Bmem cells demonstrated that lineages found in D7 T-bet^{+}FcRL5^{+} and T-bet^{neg}FcRL5^{neg} could persist for at least 120 days (Fig. 1F–G). Thus, both populations, while phenotypically distinct, exhibited attributes of Ag-experienced Bmem cells.

Next, we determined the size of the D7 Bmem cell subsets in each vaccinated individual and found no correlation between the frequencies of the two populations within the same HD (Fig. 1H–I). We then used the V_H BCR repertoire data to evaluate lineage sharing within the B cell subsets (Table S1). As expected, the IIV-induced D7 FcRL5^{+} and FcRL5^{neg} memory subsets had fewer lineages and were less diverse than naïve B cells (Fig. 1J), as indicated by a lower Diversity Index value[16]. Analysis of BCR lineages shared between the different B cell populations revealed minimal clonotypic overlap between naïve B cells and either Bmem cell subset (0.05%). By contrast, 2–6% of the lineages found in one Bmem cell subset were shared with the other Bmem cell subset (Fig. 1K), however many of the larger lineages found in each memory population were distinct (Fig. S1N). Thus, these two Bmem cell populations did not appear to be coordinately regulated.

IgD^{neg} HA-specific FcRL5^{+} and FcRL5^{neg} Bmem cells represent molecularly distinct populations.

Since the FcRL5^{+} and FcRL5^{neg} Bmem cell populations differed in expression of the transcriptional and epigenetic regulator T-bet[17], we performed RNA-seq and ATAC-seq analyses on D7 post-IIV sort-purified naïve B cells, PBs and IgD^{neg} H1-specific FcRL5^{+} and FcRL5^{neg} Bmem cells. We identified 1923 differentially accessible chromatin regions (DAR) and 762 differentially expressed genes (DEGs), including *FCRL5* and *TBX21* (Fig. S2A), between the FcRL5^{+} and FcRL5^{neg} subsets. Using Principal Component Analysis (PCA) to compare the transcriptomes (Fig. 2A, Table S2) and epigenomes (Fig. 2B, Table S3) of these different populations, we observed that the naïve and Bmem cell populations separated from PBs on the PC1 axis of both PCA plots (Fig. 2A–B). Consistent with this, cell cycle genes (Fig. 2C, Fig. S2B, Table S2) and the ASC-defining TFs *PRDM1*, *XBP1* and *IRF4* (Fig. 2D–F) were highly expressed by the D7 PBs but not by the other populations. Neither FcRL5^{+} nor FcRL5^{neg} Bmem cells exhibited increased chromatin

accessibility (Fig. 2G) surrounding genes that are expressed specifically in ASCs and directly regulated by IRF4[18]. Moreover, Gene Set Enrichment Analysis (GSEA) revealed no enrichment (Fig. 2H) for expression of these IRF4-controlled ASC-specific genes in the transcriptomes of either the FcRL5^{+} or FcRL5^{neg} IgD^{neg} H1-specific B cells. Likewise, Page Rank (PR)[19], which integrates transcriptional and epigenetic data sets (Table S2), predicted IRF4, PRDM1 and XBP1 as regulatory hubs of D7 PBs but not D7 FcRL5^{+} or FcRL5^{neg} Bmem cells (Fig. 2I–J).

Our data from the D7 FcRL5^{+} Bmem cells appeared at odds with a previous publication[14], which reports that the phenotypically similar D14 post-IIV CD27^{+}IgD^{neg}CD21^{lo} cells express IRF4 and BLIMP1. Our own analysis of their data (Fig. S2C) also showed enriched expression of IRF4-controlled ASC-specific genes by the D14 post-vaccination CD27^{+}CD21^{lo} Bmem cells. Since the prior study[14] examined the bulk CD27^{+}CD21^{lo} Bmem population, which contained both T-bet^{+} and T-bet^{neg} cells, on D14 post-IIV, we tested whether the IgD^{neg} HA-specific FcRL5^{+} T-bet expressing Bmem cells also upregulated the ASC transcriptional program by D14 after IIV. Upon comparing the DEG list between D14 HA-specific FcRL5^{+} and FcRL5^{neg} Bmem cells with the DEG list from the published D14 CD21^{hi} and CD21^{lo} total Bmem cells[14], we observed limited (<13%) overlap (Fig. S2D) with no evidence that IRF4, PRDM1 or XBP1 were functioning as regulatory hubs in in either D7 or D14 FcRL5^{+} Bmem cells (Fig. S2E–I). Therefore, we concluded that the IIV-elicited FcRL5^{+} T-bet-expressing HA^{+} Bmem cells were not transcriptionally committed to the ASC fate.

Next, we utilized a single cell approach to address whether the T-bet^{+} FcRL5^{+} Bmem cell subset could be identified in a marker agnostic non-supervised fashion,. Unlike a recent single cell RNA analysis[13], which identified 2 Bmem cell clusters following prime boost with a neo Ag (H7N9), our analysis of IIV-elicited single cell-sorted HA-specific IgD^{neg} B cells revealed 7 clusters (Fig. 2K), including 5 clusters (C0-C4) with sufficient cells for detailed analysis (Table S4). Clusters C0, C1 and C2 contained IgM^{+} cells with fewer somatic mutations as well as isotype-switched cells that were more extensively mutated (Fig. 2L). Clusters C3 and C4 were almost entirely isotype-switched (Fig. 2L). C3 contained both heavily mutated switched cells as well as less mutated switched cells, while the C4 switched cells were all extensively mutated (Fig. 2L). Clusters C0, C1, and C2 contained very few *TBX21*-expressing cells, while clusters C3 and C4 included most of the *TBX21*-expressing (Fig. 2M) and FcRL5^{+} (Fig. 2N, Table S4) cells. Next, we defined the unique DEG (Table S4) for each cluster and used GSEA to compare these DEGs with the rank gene list derived from the bulk RNA-seq analysis of sort-purified D7 HA-specific IgD^{neg} FcRL5^{+} and FcRL5^{neg} Bmem cells. DEGs from C1 were not enriched in either the FcRL5^{+} or FcRL5^{neg} Bmem cell subsets (Table S4). C0 and C2 were transcriptionally enriched for genes that are more highly expressed by the FcRL5^{neg} Bmem cell subset while C3 and C4 were transcriptionally enriched for genes upregulated in the FcRL5^{+} Bmem cell subset (Fig. 2O–P). Thus, the analyses of IIV-induced HA^{+} Bmem cells as single cells or as phenotypically defined subsets supported the conclusion that FcRL5^{+} T-bet-expressing Bmem cells are molecularly distinct from FcRL5^{neg}T-bet^{neg} Bmem cells.

IgD^{neg} HA-specific Bmem cells can be subdivided into stable effector-like and stem-like populations.

Since T-bet regulates effector function in other immune cell types[20], we hypothesized that FcRL5 and *TBX21*-expressing HA-specific Bmem cells might exhibit transcriptional features of effector cells. Consistent with this, we found that known central memory T cell genes[21] like *CCR7*, *BCL2* and *TCF7*, were downregulated in the FcRL5^{+} Bmem cells while known effector memory T cell genes[21], like *TBX21*, *ZEB2* and *CXCR3,* were upregulated in FcRL5^{+} Bmem cells (Fig. 3A). GSEA also revealed enriched expression of effector T cell genes[22,23] within the *TBX21*$^{+}$ FcRL5^{+} Bmem cell compartment (Fig. 3B). Next, we used PR (Table S2) to identify TFs predicted to regulate the gene networks in D7 post-IIV HA-specific FcRL5^{+} relative to FcRL5^{neg} Bmem cells. Again, we observed that effector-associated TFs[7,8], like T-bet, BATF and BHLHE40, were predicted to regulate the FcRL5^{+} Bmem cell transcriptional gene network while central memory-associated TFs[6,24], like TCF7 and LEF1, were predicted to regulate the FcRL5^{neg} Bmem cell gene network (Fig. 3C).

These data were consistent with the possibility that FcRL5^{+} Bmem cells represented recently activated memory cells while FcRL5^{neg} Bmem cells were more mature and would accumulate with time after vaccination. If so, we predicted that we would observe a shift of the D7 FcRL5^{+} clonotypes into the D14 FcRL5^{neg} population (Table S1). However, D7 FcRL5^{+} B cell lineages were more represented in the D14 FcRL5^{+} population relative to the D14 FcRL5^{neg} subset (Fig. 3D). Similarly, we observed more connections between the D14 and the D28 FcRL5^{+} subsets than between the D14 FcRL5^{+} and D28 FcRL5^{neg} subsets (Fig. 3E), even when rarefaction analysis was performed to control for the number of compared lineages. These results were further supported by PR (Table S2), which predicted that T-bet, BATF and BHLHE40 serve as regulatory hubs of both D7 and D14 FcRL5^{+} Bmem cells (Fig. 3F). Thus, the *TBX21*-expressing FcRL5^{+} memory population was not a transient intermediate but rather appeared to be a stable Bmem cell subset endowed with an effector-like molecular program.

T-bet associated transcriptome and epigenetic changes distinguish effector and resting Bmem cell programs.

Since PR predicted T-bet as a regulator of 991 genes in the FcRL5^{+} Bmem cell subset (Table S2), we assessed whether T-bet might contribute to the transcriptional and epigenetic landscape of FcRL5^{+} Bmem cells. Using the ATAC-seq data, we observed that chromatin accessibility surrounding HOMER-defined T-bet binding motifs was differentially enriched in the FcRL5^{+} subset relative to FcRL5^{neg} Bmem cells and PBs (Fig. 4A). Similarly, previously described T-bet ChIP-seq peaks[25] were more accessible in the FcRL5^{+} Bmem cells (Fig. 4B). Next, we identified genes encoding TFs that were differentially expressed between FcRL5^{+} and FcRL5^{neg} Bmem cells and were also assigned to at least one T-bet binding motif containing DAR and/or T-bet ChIP-seq peak (Fig. 4C, Table S3). We observed that expression of multiple TFs changed progressively between FcRL5^{neg} cells, FcRL5^{+} cells and ASCs (Fig. 4C). For example, *TCF7*, which is reported to support stem-like potential in memory T cells[6] and *BACH2*, which maintains B lineage identity[9] and prevents ASC development[10,11], were both more highly expressed in the FcRL5^{neg} subset and

decreased progressively in the FcRL5$^+$ cells and ASCs (Fig. 4D–E). The FcRL5$^+$ subset and ASCs also exhibited decreased chromatin accessibility in *TCF7* and *BACH2* associated DARs containing T-bet binding sites (Fig. 4D–E). By contrast, ASC-associated TFs, like *TOX2* and *ARID3A,* were more highly expressed in the FcRL5$^+$ subset relative to the FcRL5^{neg} subset and chromatin accessibility within the *TOX2* and *ARID3A* assigned DAR with T-bet binding sites was increased (Fig. 4F–G). Thus, T-bet expression by FcRL5$^+$ Bmem cells was associated with epigenetic and transcriptional changes that favor an effector-like program.

TBX21-expressing FcRL5$^+$ HA-specific Bmem cells exhibit distinct metabolic and signaling profiles.

Our prior GSEA (Fig. 3B) revealed that D7 FcRL5$^+$ Bmem cells were enriched for expression of genes associated with T effector cells, particularly genes that regulate metabolism and protein production. To assess whether specific metabolic programs were transcriptionally enriched in the FcRL5$^+$ *TBX21*$^+$ Bmem cells subset, we performed GSEA with the curated Gene Ontology (GO) mSigDB gene set collection[26]. Although none of the GO gene sets were enriched within the FcRL5^{neg} Bmem cell dataset, 185 GO gene sets were both enriched and upregulated in the FcRL5$^+$ Bmem cell transcriptome (Table S2). We used the leading-edge gene lists from the 185 GO gene sets to cluster the gene sets with the most similar leading-edge gene lists (Table S2, Fig. 5A). Next, we selected 11 representative GO mSigDB gene sets ((Prototypic genesets *i-xi*), Fig. S3A, Table S2) and performed PCA using the leading-edge genes from each prototypic gene set. We observed that expression of the leading-edge gene sets from these 11 prototypic GO gene sets differed substantially between FcRL5$^+$ and FcRL5^{neg} HA-specific Bmem cell subsets on both D7 and D14 (Fig. 5B).

We then used the functional annotations of the leading-edge genes from the 11 prototypic GO gene lists to group the genes into signaling and metabolic genes modules (Table S2). The genes in all 14 modules were upregulated by the FcRL5$^+$ Bmem cells. These included BCR and cytoskeleton assembly and signaling genes (Modules 1–2, Fig. 5C, Fig. S3B–C) and genes involved in endosome and lysosome cargo trafficking, autophagosomes, lysosome function and the lysosome-associated mTORC1 signaling complex (Modules 3–6, Fig. 5C, Fig. S3D–G). Moreover, we consistently observed that programs regulating mitochondrial activity and ATP metabolism, including the electron transport chain (ETC), oxidative phosphorylation, the tricarboxcyclic acid (TCA) cycle and mitochondrial fatty acid β-oxidation (FAO), were activated in FcRL5$^+$ Bmem cells (Modules 7–10, Fig. 5C, Fig. S3H–K). We noted that FcRL5$^+$ Bmem cells upregulated genes associated with producing and degrading toxic[27] reactive oxygen species (ROS). We observed that FcRL5$^+$ Bmem cells had increased expression of genes associated with caspase-dependent and independent apoptosis as well as genes associated with detoxifying free radicals (Modules 11–12, Fig. 5C, Fig. S3L–M). These included genes in the pentose phosphate pathway (PPP), which is required for de-toxification of free radicals and biosynthesis of purines and FAs (Module 13, Fig. 5C, Fig. S3N). Finally, we found genes involved in protein production and catabolism, including components of the ER associated degradation complex (ERAD)[28] and proteasome subunits, were upregulated in FcRL5$^+$ Bmem cells (Fig. 5C Module 14, Fig. S3O). To

assess whether these metabolic programs were stable attributes of the FcRL5$^+$ Bmem cells, we performed PCA using the 14 module gene sets and observed that the these metabolic programs were also enriched in D14 FcRL5$^+$ Bmem cells (Fig. 5D). Finally, using independently curated gene lists for each of these metabolic pathways in GSEA, we observed that the D7 FcRL5$^+$ Bmem cell transcriptome was enriched for mTORC1 signaling genes (Fig. 5E), fatty acid metabolism (Fig. 5F), mitochondrial metabolism (Fig. 5G), oxidative stress (Fig. 5H), and the proteasome (Fig. 5I). These data therefore suggested that the HA-specific FcRL5$^+$ Bmem cell subset represented a metabolically distinct effector-like population.

FcRL5$^+$ Bmem cells are metabolically poised and rapidly differentiate.

To assess whether the metabolic transcriptional programs correlated with the metabolic activity of FcRL5$^+$ Bmem cells, we performed *in vitro* functional assays. Since the number of circulating Ag-specific Bmem cells was limiting for most functional analyses, we evaluated the FcRL5$^+$ and FcRL5^{neg} CD27$^+$IgD^{neg} Bmem cells found in adult human lymphoid tissues[29]. Using FcRL5 to subdivide the tissue-residing CD27$^+$ Bmem cells into T-bet expressing (FcRL5$^+$) or T-bet non-expressing (FcRL5^{neg}) populations (Fig. S4A–C), we stained the cells with H_2DCF (Fig. 6A, Fig. S4D), mitotracker green (Fig. 6B, Fig. S4D) or BODIPY 510 (Fig. 6C, Fig. S4E) and measured intracellular ROS activity, mitochondrial mass and fatty acid metabolism. In each case, staining was increased in the tonsil CD27$^+$ FcRL5$^+$ Bmem cells. Moreover, tonsil FcRL5$^+$ Bmem cells exhibited increased phosphorylation of the mTORC1 target, S6 kinase (Fig. 6D, Fig. S4D). Thus, tonsil CD27$^+$FcRL5$^+$ Bmem cells displayed metabolic attributes that were congruent with the metabolic profiles identified in the transcriptome of vaccine-elicited FcRL5$^+$ Bmem cells.

As B cells transition into ASCs, the cells undergo major metabolic reprogramming to support high rate Ab production and secretion[30]. These metabolic shifts include increasing oxidative phosphorylation[31] and mTORC1 activity[32] and adapting to increased cellular and ER stress through ROS detoxification mechanisms[27,33] and the unfolded protein response (UPR)[28]. To assess whether FcRL5$^+$ Bmem cells, which have already upregulated many of these metabolic programs, are poised to rapidly differentiate into ASCs following re-activation, we stimulated CellTrace Violet (CTV)-labeled purified tonsil-derived B cell subsets for 3 days with TLR7/8 ligand, IFNγ, IL-2 and IL-21. To ensure that the cultures were not contaminated with the previously described[34] IgD^{neg}CD27^{neg} FcRL5$^+$ B cells that already express the ASC commitment factors BLIMP1 and IRF4, we focused first on comparing FcRL5$^+$ IgD^{neg}CD27$^+$ Bmem cells to naïve B cells and FcRL5^{neg} IgD^{neg}CD27$^+$ Bmem cells. Approximately half of the naïve B cells died in culture within the first 2 days (Fig. 6E) and the cells that remained did not divide (Fig. 6F) or differentiate (Fig. 6G–I). While fewer tonsil FcRL5$^+$ Bmem cells survived when compared to the matched FcRL5^{neg} population (Fig. 6E), the surviving FcRL5$^+$ Bmem cells divided at least once within 48 hours while the FcRL5^{neg} cells remained undivided (Fig. 6F). Moreover, while very few ASCs were found in day 2 FcRL5^{neg} Bmem cells cultures, ASCs were easily detected in matched day 2 FcRL5$^+$ Bmem cell cultures (Fig. 6G–I). By day 3, ASCs were detected in the FcRL5^{neg} Bmem cell cultures, however ASC formation was still less than

that seen in day 3 FcRL5^{+} Bmem cell cultures (Fig. S4H–L). Next, we asked whether the FcRL5^{+} IgD^{neg}CD27^{+} Bmem cells differentiated at similar rates to the previously described[34] IgD^{neg}CD27^{neg} FcRL5^{+} committed pre-ASCs. Again, we observed that the FcRL5^{neg}CD27^{+} Bmem cells did not efficiently differentiate into ASCs within 2 days. By contrast, both the FcRL5^{+}CD27^{+} Bmem cells and the IgD^{neg}CD27^{neg}FcRL5^{+} pre-ASCs differentiated efficiently into ASCs (Fig. S4M–N). These data therefore suggested that the T-bet expressing FcRL5^{+}CD27^{+} Bmem cells from the tonsil exhibited effector-like metabolic properties and were poised to rapidly proliferate and differentiate into ASCs.

Vaccine-specific T-bet^{+} Bmem cells produce intracellular Ig.

Data from mouse B cells[35] demonstrate that UPR genes associated with B cell activation (B cell activity UPR) and early initiation of the ASC program (PC-inductive UPR) are induced in a XBP1-independent and mTORC1-dependent fashion. Using GSEA, we observed enrichment of both the B cell activity and PC-inductive UPR program in the D7 vaccine-elicited FcRL5^{+} Bmem cells (Fig. 6J–K, Fig. S5A), suggesting that these cells have upregulated metabolic programs necessary for ASC effector function.

Another feature associated with the early ASC transition[30] is the switch from production of membrane-associated Ig (extracellular (EC) Ig) to secreted Ig (intracellular (IC) Ig). We therefore examined surface Ig expression in the Bmem cell subsets (Fig. 6L) and observed that the mean fluorescence intensity (MFI) of HA tetramer binding to the IgD^{neg} T-bet^{+} cells was decreased (HA^{int}) relative to that seen in the IgD^{neg} T-bet^{neg} B cells (HA^{hi}). This finding was not unique to our vaccine cohort as HA^{int} cells have been observed in other studies[2] (Fig. S5B). To ensure that the lower HA-binding seen in the FcRL5^{+} T-bet^{+} Bmem cells was not due to differences in the affinity of the BCRs expressed by these cells, we generated recombinant IgG1 mAbs, which were single-cell cloned from D7 FcRL5^{+} HA^{int} and FcRL5^{neg} HA^{hi} Bmem cells, and measured the binding of these mAbs to recombinant HA protein. As we observed no significant differences in binding avidity between the Abs derived from the two Bmem cell populations (Fig. S5C–D, Table S5), we next used anti-IgG and anti-IgA reagents to quantify surface Ig expressed by the Bmem cells (Fig. 6M). This analysis, which detected the constant region of the plasma membrane-associated EC Ig and did not rely on binding to the V_H domain, again indicated that the FcRL5^{+} T-bet-expressing Bmem cells expressed less membrane-associated Ig.

Given the reduction in Ig surface expression by the FcRL5^{+}T-bet^{+} Bmem cells, we next measured class-switched IgH transcript expression. Although we observed no significant differences in IgH transcript expression by the two HA-specific Bmem cell populations (Fig. 6N), we found that the ratio of transmembrane exon transcripts to IgG secretory exon transcripts was lower in D7 FcRL5^{+} Bmem cells (Fig. S5E). We next used ImageStream to measure HA-specific EC Ig and IC Ig in sort-purified D7 IgD^{neg} B lineage cells. We identified CD38^{hi} PBs that expressed abundant IC H1-specific Ig (Fig. 6O–P) and minimal EC H1-specific Ig (Fig. 6O, Q). The T-bet^{neg} Bmem cells exhibited high expression of EC H1-specific Ig and low to undetectable expression of IC H1-specific Ig (Fig. 6O–Q). By contrast, T-bet^{+} H1-specific Bmem cells exhibited low expression of EC H1-specific Ig (Fig. 6O, Q) but measurable expression of IC H1-specific Ig (Fig. 6O–P). Moreover, the ratio

of EC/IC H1-binding was lower in the T-bet^{+} Bmem cells relative to the T-bet^{neg} Bmem cells (Fig. 6R). Thus, the vaccine-induced FcRL5^{+} effector-like Bmem cell subset appeared poised to produce secretory Ig.

The T-bet^{+} Bmem cell subset contributes to secondary ASC responses and predicts enduring humoral immunity to IIV.

T cell effector memory declines more rapidly than lymphoid tissue-associated central memory[36]. To assess the durability of the vaccine-elicited FcRL5^{+} Bmem cell population, we vaccinated HD over two sequential seasons with vaccines that contained the same H1 (2015 and 2016) or H3 Ag (2016 and 2017) (Fig. 7A). On D7 post-vaccination each year, we determined the frequency of T-bet^{+} and T-bet^{neg} Bmem cells specific for the HA Ag that was conserved in the vaccine across consecutive years. On D7 post-immunization with the 2015 influenza vaccine (Fig. 7A), we identified both T-bet^{+} and T-bet^{neg} CA09(H1)-specific B cells (Fig. 7B). Following revaccination in 2017, the frequency of T-bet^{neg} CA09(H1)-specific Bmem cells remained constant while the T-bet^{+} fraction declined (Fig. 7B). Similar results were seen (Fig. 7C) when we compared B cells responses to HK14(H3) in 2016 and 2017. Compilation of the reactivity data across 11 HDs revealed a selective reduction in the D7 T-bet^{+} vaccine-specific Bmem cell subset between years 1 and 2 following repeat vaccination with the same Ag (Fig. 7D).

The loss of the T-bet^{+} Bmem cell population following consecutive vaccinations might reflect a shorter lifespan for these cells or could imply that the T-bet^{+} Bmem cells differentiate into PBs following Ag re-exposure. To test the latter, we purified the D7 or D14 FcRL5^{+} and FcRL5^{neg} HA-specific Bmem cells from three HDs and then reimmunized those individuals a year later with a vaccine containing the identical H3 Ag and a very similar H1 Ag (97.4% identity). We isolated the circulating D7 PBs following the second vaccination and compared the BCR repertoire between the year 1 Bmem cells and year 2 PBs. We identified shared lineages between the year 1 FcRL5^{+} Bmem cells and the year 2 PBs in all three HDs (Fig. 7E–G, Table S1). In two HDs we identified multiple lineages that exhibited 100% identical VDJ nucleotide sequences between the year 1 D7 Bmem cells and the year 2 D7 PBs. Moreover, in all 3 HDs we observed more lineage sharing between the year 1 FcRL5^{+} Bmem cells and the year 2 PBs relative to the sharing seen between year 1 FcRL5^{neg} Bmem cells and year 2 PBs. While the increased frequency of sharing between the year 1 FcRL5^{+} Bmem cells and the year 2 PBs did not quite reach significance ($p=0.058$), the data showed that cells from the D7 FcRL5^{+} and FcRL5^{neg} Bmem cell compartments can persist for a year and that the FcRL5^{+} Bmem cell subset may exhibit enhanced capacity to contribute to the rapid Bmem cell-derived ASC recall response.

Since some FcRL5^{+} Bmem cells and FcRL5^{neg} Bmem cells were long-lived, we asked whether their presence on D7 post-vaccination correlated with the development of the long-lived systemic Ab response following vaccination. We therefore determined the fold-change in the vaccine-specific H1 and H3 IgG Ab response between D0 and D120 post-immunization in 19 vaccinated HD and compared this response to the size of the D7 PB, T-bet^{+} and T-bet^{neg} H1-specific or H3-specific Bmem cell responses in those individuals. As previously reported[37], the early circulating PB response did not correlate with the

long-lived humoral immune response (Fig. S6A). Similarly, we observed no correlation between the fold-increase in systemic Ab responses 4 months after vaccination and the size of the T-bet^{neg} H1-specific or T-bet^{neg} H3-specific populations on D7 (Fig. 7H–I) or D14 (Fig. S6B–C) post-vaccination. However, we observed a positive correlation between the size of the T-bet^{+} H1-specific and T-bet^{+} H3-specific Bmem cell subsets on D7 (Fig. 7J–K) and D14 (Fig. S6D–E) and the magnitude of the D120 H1- or H3-specific humoral immune response. This effect was Ag specific as no correlation was seen between the T-bet^{+} H1-specific Bmem cell response and the change in H3 Ab titers or vice versa (Fig. S6F–G). Thus, the T-bet^{+} FcRL5^{+} metabolically poised Bmem cells exhibit transcriptional, epigenetic and functional attributes of effector Bmem (eBmem) cells and these cells not only persist but may represent an early predictive biomarker of long-lived humoral immunity to seasonal IIV.

Discussion

Using standard phenotypic profiling approaches and marker-agnostic single cell methods, we demonstrated that IIV elicits IgD^{neg}CD27^{+} FcRL5^{+} T-bet-expressing Bmem cells that are isotype-switched and somatically hypermutated. D7 FcRL5^{+}T-bet^{+} HA-specific Bmem cells shared some phenotypic and transcriptional attributes with other previously described vaccine-elicited B cell populations, including the CD27^{neg}IgD^{neg} HA-specific newly generated Bmem cells[13] and the D14 post-IIV CD27^{+}CD21^{lo} pre-ASCs[14]. However, transcriptional and epigenetic profiling of the HA-specific FcRL5^{+} cells revealed that these cells were distinct from the previously described memory populations and share transcriptional attributes also seen in effector and effector memory CD8^{+} T cells. Whether the phenotypic characteristics of the FcRL5^{+} cells remain static or change with time, as previously reported for mouse Bmem cells[38], is unclear. Regardless, we observed FcRL5^{+} T-bet^{+} HA-specific Bmem cells circulating for at least 4 months following vaccination in humans. We also found clonotypes from day 7 FcRL5^{+} cells recalled to the PB compartment after re-vaccination one year later. Thus, the FcRL5^{+} Bmem cells were not simply recently activated effectors that rapidly disappeared but instead represented *bona fide* memory cells.

Effector memory CD8^{+} T cells are distinguished by changes in cellular metabolism, respiration and mitochondrial dynamics[39]. Consistent with this, we found FcRL5^{+} HA-specific Bmem cells also increased expression of genes linked to energy intensive metabolic processes like protein and macromolecule synthesis. Similar metabolic programming changes are seen in ASCs[40] and are required for the development of fully functional ASCs[31 41]. These metabolic changes necessitate adjustment to the ER stress from misfolded proteins in a process referred to as the unfolded protein response or UPR[28]. In ASCs, the UPR is induced and maintained by the TFs IRE1, XBP1 and ATF6[28] and is associated with the downregulation of PERK[42]. Even though the FcRL5^{+} Bmem cells downregulated PERK (*EIF2AK3*) and increased expression of UPR and ERAD-associated genes, like *OS9*, *UBA1* and *VCP*, these cells did not up-regulate *XBP1*, *IRE1* or *ATF6*, suggesting that FcRL5^{+} Bmem cells regulate cellular stress responses through an XBP1-independent mechanism. A recent publication[35] reported that UPR-associated genes are upregulated following B cell activation and before ASC commitment in an XBP1-independent and mTORC1 dependent manner. Consistent with this publication, we observed that tonsil-derived FcRL5^{+} Bmem cells showed increased basal mTORC1 activity and that vaccine-elicited FcRL5^{+}

Bmem cells had increased expression of mTORC1 complex genes, including *LAMTOR1*, *LAMTOR2* and *LAMTOR5*. The modified metabolism of the FcRL5$^+$ Bmem cell subset appeared to support increased protein synthesis and engage the compensatory programs necessary for sustained protein production as we observed that the ratio of intracellular Ig to membrane-associated Ig shifted in favor of intracellular Ig in the HA-specific T-bet$^+$ Bmem cells. Thus, we postulate that the constitutive production of intracellular Ig poises T-bet expressing FcRL5$^+$ cells to rapidly produce secreted Ab once ASC commitment transcription factors, like BLIMP1, are induced following reactivation. Based on these data and analogous to effector memory CD8$^+$ T cells, which are also poised to secrete effector proteins upon reactivation, we argue that the IIV-induced T-bet expressing FcRL5$^+$ Bmem cell population represents an effector Bmem (eBmem) cell subset.

We cannot say from our study whether T-bet controls the development or function of IIV-elicited eBmem. However, PR[19], which integrates transcription and chromatin accessibility data, predicted T-bet as an upstream regulator of >900 genes in the FcRL5$^+$ eBmem cell gene network and T-bet was linked to chromatin remodeling in FcRL5$^+$ eBmem cells. Moreover, *BACH2*, which must be turned off during ASC commitment[10,11], showed loss of chromatin accessibility surrounding T-bet binding sites and was downregulated in FcRL5$^+$ Bmem cells. By contrast, chromatin accessibility surrounding T-bet binding sites was increased in the *TOX2* and *ARID3A* loci and expression of these genes was higher in FcRL5$^+$ eBmem cells. Given that TOX2 supports chromatin accessibility[43] and ARID3A is a transactivator of IgH locus[44] these data suggest that T-bet has the potential to contribute to the epigenetic changes that support fate decisions and effector functions of the FcRL5$^+$ eBmem cell subset.

Finally, our data showed that the size of the D7 post-IIV T-bet$^+$ eBmem cell response positively correlated with the development of a long-lived serum Ab response. This correlation does not imply that T-bet$^+$ Bmem cells are recent GC emigrants or precursors of long-lived ASCs but does suggest that the signals required to elicit the early T-bet$^+$ eBmem cell response may also be involved in the development of a durable ASC response. This finding is important because flow-based assays that can be used early after vaccination to predict long-lived humoral B cell immunity to IIV are lacking[45,46]. Thus, the IIV-elicited FcRL5$^+$T-bet$^+$ eBmem cell subset represents a pool of memory cells that has the potential to quickly contribute to the rapid burst of secreted Ab following re-exposure to the same or closely related Ags. In addition, the quick induction of the FcRL5$^+$ T-bet expressing Bmem cells following IIV may represent an easily monitored cellular compartment that can be used to predict the development of long-lived Ab responses to IIV.

Limitations of the study.

Our data did not directly test whether T-bet regulates the development or function of HA-specific eBmem cells. Our data did not demonstrate that vaccine-elicited T-bet expressing Bmem cell population can serve as correlate of protection from disease following influenza exposure. Finally, we do not know whether the T-bet$^+$FcRL5$^+$CD27$^+$ Bmem cell subset is induced in response to other vaccines or whether the presence of these eBmem cells can be used to predict the durability of the humoral response to other vaccines.

STAR Methods

RESOURCE AVAILABILITY

LEAD CONTACT—Further information and requests for resources and reagents should be directed to and will be fulfilled by the Lead Contact, Frances E. Lund, flund@uab.edu

MATERIALS AVAILABILITY

Reagents generated in this study include recombinant HA proteins that were tetramerized for flow cytometry analyses, used in ELISA assays and conjugated to beads for cytometric assays. DNA constructs used to generate the recombinant proteins are freely available upon request. Recombinant HA-specific monoclonal Abs were cloned from single Bmem cells. DNA expression constructs for these recombinant Abs are also available upon request.

DATA AND CODE AVAILABILITY

- Sequencing data have been deposited in the NCBI Gene Expression Omnibus (GEO) and are publicly available as of the date of publication. Accession numbers are listed in the Key Resources Table.
- All original code has been deposited at Zenodo. DOIs are listed in the Key Resource Table.
- Any additional information required to reanalyze the data reported in this paper is available from the lead contact upon request.

EXPERIMENTAL MODEL AND SUBJECT DETAILS

Experimental models and subject details.—The UAB Institutional Review Board approved all human study protocols. Subjects, who self-identified as healthy, were recruited and provided informed consent through the Alabama Vaccine Research Clinic (AVRC). Twenty-seven subjects were recruited into the study across sequential vaccine seasons (2015–2019). The mean age was 30. Fifty-eight percent of these subjects were male and forty-two percent of these subjects were female. Sixty-three percent of these subjects were Caucasian and thirty-seven percent of these subjects were African-American. Subjects received 2015–2016 Fluzone (Sanofi-Pasteur), 2016–2017 Fluvirin (Sequiris), 2017–2018 Fluzone (Sanofi-Pasteur), 2018–2019 Fluzone (Sanofi-Pasteur) or 2020–2021 Fluzone (Sanofi-Pasteur). Blood was drawn on days 0, 7, 14, 21, 28 and 120 days +/− 1 week. The O'Neal Comprehensive Cancer Center Tissue Procurement Shared Facility provided remnant tonsil tissue samples from de-identified patients undergoing routine tonsillectomies.

METHOD DETAILS

Lymphocyte and plasma isolation.—Peripheral blood from human subjects was drawn into K2-EDTA tubes (BD Bioscience). Peripheral blood mononuclear cells (PBMCs) and plasma were isolated by density gradient centrifugation over Lymphocyte Separation Medium (CellGro). Red blood cells were lysed with ammonium chloride solution (StemCell). Plasma and PBMCs were either used immediately or aliquoted and stored at −80°C.

Flow Cytometry.—Single cell suspensions were blocked with 2% human serum and stained with Ab panels described in Table S5. 7AAD or LIVE/DEAD Fixable Dead Cell Stain Kits (Molecular Probes/ThermoFisher) were used to discriminate live cells. To detect HA-specific B cells, cells were treated at 37°C with 0.5U/ml neuraminidase (*C. perfringens*, Sigma) to remove sialic acid, and were washed, blocked and stained with HA tetramers. Intracellular proteins were detected by staining with Abs specific for cell surface markers, fixing the cells in 10% neutral buffered formalin solution (Sigma), and then staining the permeabilized cells (0.1% IGEPAL (Sigma)) with Abs or fluorochrome-labeled HA tetramers. Stained cells were analyzed using a FACSCanto II (BD Bioscience) or the Attune NxT flow cytometer (Invitrogen, ThermoFisher). FlowJo v9.9.3 or FlowJo v10.2 were used for analysis.

Cell Sorting.—B cell subsets were sort-purified for BCR-seq, RNA-seq, ATAC-seq, rMAb generation, Mitotracker green assays, mTORC1 pS6 assays and *in vitro* culture experiments with a FACSAria (BD Biosciences) or Melody (BD Biosciences) in the UAB Comprehensive Flow Cytometry Core. Table S5 shows flow panels used for subset sort-purifications.

BCR repertoire library preparation and informatics.—B cell subsets were sorted directly into RLT buffer and snap frozen in LN_2. RNA was extracted using the quick start protocol from QIAGEN RNeasy Mini Kit. First strain cDNA synthesis was performed using iScript cDNA synthesis kit (BioRad) and 8 μl of RNA. First round amplification of IgG, IgA, and IgM was performed in 25 μl reaction volume using 4–8 μl cDNA, Platinum PCR SuperMix High Fidelity (Invitrogen), and 1μl gene specific primers (120 nM) of VH1-VH7 FR1 (forward) and Ca, Cu, Cg (reverse) [16]. First round PCR conditions were: 95°C for 3 min, 42 cycles of 30s 95°C, 30s 58°C, 30s 72°C, and 72°C for 3 min. PCR products were verified on 1.2% agarose gels and then indexed in a 2nd round PCR reaction using the Nextera Index kit (Illumina). PCR2 conditions for indexing were: 72°C for 3 min, 98°C for 30s and 5 cycles of 98°C for 10s, 63°C for 30s, and 72°C for 3 min. Indexed PCR products were purified with Agencourt AMPure XP beads (Beckman), quantitated by NanoDrop and then pooled into libraries. Libraries were denatured using 0.2N NaOH and quenched with cold HT1 per manufacturer (Illumina) instructions. Denatured libraries were diluted with 20% PhiX (Illumina) as an internal quality control and loaded onto a 600-cycle V3 MiSEQ cartridge (Illumina) for sequencing.

Ig V_H sequencing data were processed as described previously[16]. Briefly, joined paired-end reads were assembled using Fastq-join (https://github.com/ExpressionAnalysis/ea-utils) and quality filtered. Sequences with ≤ 200bp or with low-quality bases (> 0bp with quality scores < 10, or ≥ 5bp with quality scores < 20, or ≥ 15bp with quality scores of 30) were eliminated from further analysis. Overall quality of sequences was assessed using FastQC (https://www.bioinformatics.babraham.ac.uk/projects/fastqc/). Sequences were annotated for isotype and submitted to IMGT/High V-QUEST[50] web portal for V_H-, J_H-gene annotations, alignments and tabulation of mutations. Sequences annotated as “productive” were considered for further analysis. For each donor, sequences (from all B cell subsets) were clustered into lineages based on shared rearrangements (same V_H and J_H genes,

and same HCDR3 length) as well as pairwise HCDR3 nt sequence similarity ≥ 85% (see[16] Supplementary Note 1). Mutation frequencies were determined based on non-gap mismatches of expressed sequences relative to their annotated V_H germline sequences. Downstream analysis and visualization were performed in Matlab (R2020a, The Mathworks Inc., Natick MA). BCR Rep-seq data, including both raw and selected IMGT output with lineage assignments, can be accessed SuperSeries accession GSE222476 or directly at accession GSE222474.

RNA-seq library preparation and data analyses.—B cell subsets were sorted directly into RLT buffer (Qiagen) with 1% mercaptoethanol and then snap-frozen in LN_2. RNA was extracted using the QuickRNA Micro Prep Kit (Zymo) and cDNA was prepared using SMART-seq v4 cDNA synthesis kit (Takara). Sequencing libraries were constructed using 200 pg cDNA as input for the NexteraXT kit with NexteraXT indexing primers (Illumina). Libraries were quality assessed, pooled and sequenced using 75 bp paired-end chemistry on a NextSeq500 at the UAB Helfin Genomics Core. Sequencing reads were mapped to the hg38 version of the human genome using STAR[51] with the default settings and the UCSC KnownGene table as a reference transcriptome. Reads overlapping exons were tabulated using the GenomicRanges[52] package in R/Bioconductor. Genes expressed at 3 reads per million or more in all samples from one group were considered detected and used as input for edgeR v3.24.3[53] to identify DEG. P-values were FDR corrected using the Benjamin-Hochberg method[54] with genes of an FDR <0.05 and a FC >1 or <−1 log(2) considered significant. Expression data was normalized to reads per kilobase per million mapped reads (RPKM). Samples included either four (D14 timepoint) or six (D7 timepoint) biological replicates per B cell subset. Principal component analysis was performed using the vegan package v2.5.6. Gene set enrichment analyses (GSEA) were performed by taking the ranked list (ranked by multiplying the $-\log_{10}$ of the P-value from edgeR by the sign of the FC) of detected genes in the RNA-seq datasets and as input in the GSEA[55] PreRanked analysis program (http://software.broadinstitute.org/gsea/index.jsp). Gene lists evaluated by GSEA include mSigDB curated Gene Ontogeny (GO) terms[26] version 7.0, collection C5 and selected gene sets provided in Table S2. Ig Transcript and Splicing Analysis. The locations of Ig gene segments were downloaded from IMGT for the hg38 genome and reads that overlapped each segment was calculated and RPKM normalized using the GenomicRanges[52] package in R v3.6.3. To determine the reads that mapped to the membrane or secretory specific Ig exons, a splice graph was constructed using the Ensemble hg38 transcriptome v105 and the SplicingGraphs (https://bioconductor.org/packages/SplicingGraphs) package in R v4.1.0. For each sample, the reads spanning the exon junctions between common and secreted exons or between common and membrane bound exons for all IGHG isotypes were calculated, normalized to total unique reads, and the ratio of membrane versus secreted was computed. All RNA-seq data is available from the GEO database under the accession GSE163989 and SuperSeries accession GSE222476. See also Table S2.

Identification of signaling and metabolism transcription modules in effector Bmem cells.—GSEA was performed comparing the ranked gene list of D7 post-vaccine IgD^{neg} H1-specific $FcRL5^{+}$ and $FcRL5^{neg}$ Bmem cell subsets to 3931 GO terms (mSigDB

version 7.0, collection C5). Enriched gene sets with an FDR q-value < 0.01 were identified (See Table S2). A distance matrix was constructed based on 1 - Jaccard index of the constituent leading-edge genes of pairs of these enriched terms and was used for classical multidimensional scaling to visualize the terms in three-dimensional space. Terms were grouped in clusters (k-means clustering with n=9 as specified by the gap statistic[56]) using Matlab's evalcluster function. Leading-edge genes from the GO lists present in each cluster were compared and 11 prototypic gene lists with the most similarity to other gene lists (i.e. largest number of shared leading-edge genes) within the cluster were selected (Table S2) for further analysis. The known properties of the proteins encoded by the leading-edge genes from each of the 11 prototypic GO lists were manually curated and the genes were grouped into 14 modules (Table S2) based on the reported functional and metabolic properties of proteins encoded by these genes. The module assignments were independently validated using publicly available data sets (Table S2) for the relevant metabolic pathways.

ATAC-seq preparation and analyses.—B cell subsets were enriched from PBMCs (EasySep™ Human B Cell Negative Selection Kit), sort-purified, re-suspended in 25 μl of tagmentation reaction buffer (2.5 μl Tn5, 1xTagment DNA Buffer, 0.02% Digitonin, 0.01% Tween-20) and incubated for 1hr at 37°C. Cells were lysed with 25 μl 2x Lysis Buffer (300 mM NaCl, 100 mM EDTA, 0.6% SDS, 1.6 μg Proteinase-K) for 30 min at 40°C. Low molecular weight DNA was purified by size-selection with SPRI-beads (Agencourt), and PCR amplified using Nextera primers with 2x HiFi Polymerase Master Mix (KAPA Biosystems). Amplified, low molecular weight DNA was isolated using SPRI-bead size selection. Libraries were quality assessed and sequenced using a 75bp paired end run on a NextSeq500 at the UAB Heflin Genomics Center. Raw sequencing reads were mapped to the hg38 version of the human genome using Bowtie[57] (v1.1.1) with the default settings. Duplicate reads were annotated using the Picard Tools MarkDuplicates function (http://broadinstitute.github.io/picard/) and eliminated from downstream analysis. Enriched peaks were identified using MACS2 v2.1.0.2014061) with the default settings[58]. Genomic and motif annotations were determined for ATAC-seq peaks using the HOMER[59] (v4.10) annotatePeaks.pl script. Read counts for all peaks were annotated for each sample from the bam file using the GenomicRanges[52] R/Bioconductor package and normalized to Reads Per Peak Per Million (RPPM)[60]. Differential accessible regions/peaks (DAR) were determined using edgeR v3.24.3[53] and P-values were FDR corrected using the Benjamin-Hochberg method[54]. Peaks with a >1 or <−1 log(2) FC and FDR < 0.05 between comparisons were termed significant. IRF4 target accessibility was computed by taking the mean peak accessibility for all peaks that mapped to genes derived from the Shaffer IRF4_Up in PCs dataset[18].

T-bet Motif and ChIP-seq Analysis.—T-bet motifs in accessible regions were annotated using HOMER and annotatePeaks.pl [DAR peak file] hg38 -size given -noann -m tbx21.motif -mbed [tbx21.motifs.bed]. The resulting bed file was used as input to calculate the RPPM normalized accessibility in the 50bp surrounding each motif for the indicated samples. T-bet ChIP-seq data from GM12878 cells was downloaded from the GEO database under accession GSE92020[25]. The overlap of chromatin accessibility at T-bet peaks was calculated using

the GSE92020_ENCFF971VHK_optimal_idr_thresholded_peaks_GRCh38.bed file as described above. All ATAC-seq data is available from the NCBI Gene Expression Omnibus (GEO) database under the accession GSE203112 and the SuperSeries accession GSE222476. See also Table S3.

PageRank (PR) Analysis.—PR analysis was performed using the D7 or D14 RNA-seq and ATAC-seq data sets from each subset as previously described[19]. TFs with a PR statistic greater than 0.001 in any cell type were considered for downstream analysis. The $\log_2$FC in PR statistic between subsets was calculated for each TF. See also Table S2.

Single Cell RNA-library preparation and sequencing.—Two subjects were enrolled for serial weekly blood draws one week after IIV. B cells were negative selected using column purification (EasySep Pan-B cell purification kit, StemCell Technologies), treated with neuraminidase, stained with HA tetramers, fluorophore-labeled Abs, and anti-FcRL5 Ab conjugated with TotalSeq C oligomer hashtags (Table S4). HA-specific IgD^{neg} $CD38^{lo/med}$ cells were sort-purified as described in Table S5 and bar coded. Single cell suspensions were applied to the 10XGenomics workflow for cell capture, scRNA gene expression (GEX), BCR and Feature Barcoding library preparation using the Chromium Single Cell 5' Library and Gel Bead Kit (Nest GEM 5' Kit v 1.1) as well as the Single Cell 5' Feature Barcode Library Kit (10XGenomics), following manufacturer's instructions.

Single-cell transcriptome and repertoire profiling.—Raw sequence reads were processed using CellRanger (version 5.0.0 and 5.0.1). The multi pipeline with default parameter settings was used for demultiplexing and quantifying gene expression and assembly of BCR sequences. Reference datasets used for GEX and VDJ annotation included refdata-gex-GRCh38–2020-A and refdata-cellranger-vdj-GRCh38-alts-ensembl-5.0.0 respectively (10x Genomics). Cellranger output was analyzed in R (version 3.6.3) using Seurat[61] package (version 3.2.2). Cellranger count data of the two enrolled subjects were normalized, transformed and variable genes were detected with uniform manifold approximation and projection (UMAP) performed in default parameter settings, using SCTransform, RunPCA and RunUMAP with 30 principal components. Transcriptionally similar clusters were identified with shared nearest neighbor (SNN) modularity optimization with a resolution of 0.8. High confidence V_H consensus sequences were analyzed using IMGT High-Vquest (version 3.5.21; reference release 202049–2) to retrieve VDJ annotation and nucleotide CDR3 sequence. Corresponding VDJ sequence annotation data was mapped back to known GEX barcode data for further analysis in Seurat. GSEA on single cell data was performed using the parameters 0.1 min pct, padj <0.05. scRNA-seq data can be accessed via SuperSeries accession GSE222476 or directly via accession GSE222888.

B cell *in vitro* stimulation.—Tonsil B cell subsets were sort-purified as described in Table S5 and stained for 10 min at 37°C with PBS diluted CellTrace™ Violet (Molecular Probes, Thermofisher). Labeled cells (0.5×10^6 cells/mL) were cultured for 2–3 days with 5 μg/mL R848 (InvivoGen), 50 U/mL IL-2 (Peprotech), 50 ng/mL IL-21 (Peprotech) and 20 ng/ml IFNγ (R&D) and analyzed.

HA ELISAs.—Plasma from vaccinated samples were serially diluted on EIA/RIA ELISA plates (Costar) that were previously coated with recombinant HA. HA-specific IgG Abs from the samples were detected using HRP-conjugated anti-human IgG secondary Abs (Jackson ImmunoResearch) and were developed using ABTS with acid stop. Absorbance was measured at 415nm using a SpectraMaxM2 (Molecular Devices). All samples were tested against the same reference standard and 50% endpoint titers were determined.

Metabolism assays.—Sort-purified B cell subsets (Table S5) were incubated for 15 min at 37°C with 2ng/mL of Mitrotracker Green (Invitrogen), washed in PBS and immediately analyzed or were fixed in 10% neutral buffered formalin (Sigma), permeabilized in 0.1% IGEPAL (Sigma) and stained with anti-pS6 Ab (Cell Signaling Technology). In other experiments cell, tonsil B cells were surface stained, washed and then incubated with either 2 ng/mL of H_2DFCDA (Invitrogen) for 20 min at 4°C or with 5 ng/mL of BODIPY 500/510 (Invitrogen). Cells were washed with PBS and immediately analyzed.

ImageStream.—$CD19^+$ cells were enriched (EasySep™ human B cell negative selection kit) from HD PBMCs collected D7 post-IIV. Cells were stained with APC-conjugated H1 tetramer and Abs for IgD, CD38 and CD19 for 20 min at 4°C and then fixed 10% neutral buffered formalin (Sigma). Cells were permeabilized with 0.1% IGEPAL (Sigma) in the presence of PE-conjugated H1 tetramer and anti-T-bet Ab. Cells were analyzed using ImageStreamXMarkII (Luminex) and IDEAS software. Cells were gated on in-focus singlets. The intensity mask feature was used to acquire the intensity of extracelluar H1 tetramer and intracellular H1 tetramer staining in various B cell subsets. Single cell images were exported from IDEAS software as TIFF files with direct import into CANVAS for equivalent and proportional reduction. Final images are presented as 600 dpi.

Recombinant influenza HA protein production.—The coding sequences (amino acids 18–524) of influenza HA ectodomains were synthesized (GeneArt, Regensburg, Germany) from the following influenza virus strains: A/California/VRDL7/2009 (CA09-H1), A/Switzerland/9715293/2013 (SW13-H3), A/Hong Kong/4801/2014 (HK14-H3), and A/Michigan/45/2015 (MI15-H1). As previously described[62], HA ectodomains were cloned into the pCXpoly(+) vector that was modified with a 5’ human CD5 signal sequence and a 3’ GCN4 isoleucine zipper trimerization domain (GeneArt) that was followed by either a 6XHIS tag (HA-6XHIS construct) or an AviTag (HA-AviTag construct). The HA–6XHIS and HA–AviTag constructs for each HA were co–transfected using 293Fectin Transfection Reagent into FreeStyle™ 293–F Cells (ThermoFisher Scientific) at a 2:1 ratio, respectively. Transfected cells were cultured in FreeStyle 293 Expression Medium for 3 days and the supernatant was recovered by centrifugation. Recombinant HA molecules were purified by FPLC using a HisTrap HP Column (GE Healthcare) and eluted with 250 mM imidazole.

Generation of HA tetramers and HA cytometric bead arrays.—Recombinant HA trimers were biotinylated by addition of biotin–protein ligase (Avidity). To generate HA tetramers, biotinylated HA trimers were tetramerized with fluorochrome–labeled streptavidin (Prozyme). Labeled tetramers were purified by size exclusion on a HiPrep 16/60 Sephacryl S–300 column (GE Healthcare). To generate cytometric bead arrays (CBA),

carboxy functionalized blue particle array beads (Spherotech) were directly conjugated with streptavidin (Southern Biotech) following manufacturer's protocol. Biotinylated HA tetramers were passively absorbed onto CBA particles by mixing a 5-fold excess of particle binding capacity (100 μg) of biotinylated HA with 2×10^7 Spherotech beads in 400 μl of PBS with 1%BSA. Labeled microparticles were separated by centrifugation at 3000g for 5min. HA-trimer conjugated beads were washed twice in 1ml of 1% BSA, PBS, 0.05% NaN3, resuspended at 1×10^8 beads/mL and stored at 4°C. IgG capture beads were generated by the direct conjugation of goat anti-Human IgG $F(ab)^2$ (Southern Biotech) to array particles (Spherotech) following manufacturer's protocol for direct labeling. Briefly, 2×10^7 particles were pelleted by centrifugation and resuspended in 200 μl of anti-human IgG. An equal volume of EDC (1-Ethyl-3-(3-dimethylaminopropyl)-carbodiimide), 6mg/mL, in 0.1 M MES (2-(N-morpholino) ethanesulfonic acid) buffer pH 5.0 was added and the mixture was rotated overnight at RT. Beads were washed twice by pelleting by centrifugation and resuspension in PBS. Following washing, beads were resuspended in 1% BSA in PBS with 0.005% NaN3 as a preservative.

BCR Cloning and screening of recombinant Abs.—B cell subsets were index-sorted (Table S5) and deposited as single cells into hypotonic lysis buffer in 384 well plates that were stored at −80°C. cDNA was generated using high-capacity cDNA generation kit (Roche). PCR amplicons, using forward and reverse primers specific for the amino terminus of the mature IGHV, IGKV, and IGLV proteins (Table S1), were cloned into pEGFP expression vectors that were modified to express the constant regions of human IgG1, IgKappa, or IgLambda. Plasmids encoding Ig heavy and light chain pairs were co-transfected using Polyethylenimine into 293FreeStyle cells (Invitrogen). Supernatants were assayed for secreted rAb and for HA reactivity using the HA CBA described above. The MFI of rAb binding to each HA Ag in the bead array was measured by flow cytometry (BD LSRII) and normalized for Ig by dividing the HA binding MFI by the MFI of binding to the anti-IgG capture beads (see Table S5).

Biacore Studies.—The K_D of recombinant monoclonal human Abs (rmAbs) specific for HA were determined using a T200 Biacore (GE healthcare) biosensor instrument equipped with a research grade Series S Sensor Chip SA (GE healthcare). Biotinylated recombinant CA09-H1, PR8-H1, and MI15-H1 were immobilized on the sensor following manufacturer's protocol. Binding kinetics of rmAbs were determined by monitoring association of Abs at concentrations ranging from 31.25nM to 500nM in PBS pH 7.4 for 120s then the dissociation for 600s at a flow rate of 30μl/min at 25°C. Binding surfaces were regenerated by a 60s injection of 3M MgCl. K_D values were derived from at least five concentrations in two-fold dilution series, globally fit into a 1:1 Langmuir binding model using Biacore T200 BIA Evaluation Version 1 software.

QUANTIFICATION AND STATISTICAL ANALYSES

Statistical Analyses.—Comparisons between two groups were performed with the Wilcoxson matched pairs signed rank test for non-normally distributed variables. Two-tailed t-testing was used to compare mean RPPM values for cumulative genes in the Shaffer UP in IRF4 gene set and for T-bet ChIP-seq and T-bet motif comparisons. The one-way ANOVA

test was used to compare mean values of three or more groups and either the Dunn's or Tukey's multiple comparisons test was used to compare medians. Strength and direction of association between two variables measures was performed using the D'Agostino-Pearson normality test followed by or Spearman correlation test. Data were considered significant when $P \leq 0.05$. GraphPad Prism version 7.0a or 8.0 software was used for analysis.

Other bioinformatics analyses and visualizations.—Hierarchical clustering, PCA, heatmap plots and other visualizations were created using Matlab (R2020a, The Mathworks Inc., Natick MA) or R v3.5.2.

Supplementary Material

Refer to Web version on PubMed Central for supplementary material.

Acknowledgements:

We thank the Alabama Vaccine Research Clinic and Pamela Cunningham, Heather Logan, Aeryn Peck, Catrena Johnson and Megan Oelschig for recruiting and consenting subjects. We thank Vidyasagar Hanumanthu, Director of the UAB Flow Core Facility, Dr. Michael Crowley, Director of the UAB Heflin Genomics Core, and Drs. Randall Davis and Edlue Tabengwa, Directors of the UAB Multidisciplinary Molecular Interaction Core for all their assistance with these studies. We are grateful to Dr. Amy S. Weinmann for her thoughtful commentary. Funding for the work was provided by the US National Institutes of Health (NIH): P01 AI125180 (I.S., F.E.L, J.M.B, C.D.S, E.Z.), U19 AI 109962 (F.E.L, T.D.R) and U19AI142737 (F.E.L., T.D.R., A.N., R.D.K., A.R.) A.N. received salary support from R21 AI152006, pilot grant support from the UAB AMC21 Immunology Autoimmunity and Transplantation Strategic Initiative and funding from the UAB CCTS (UL1 TR001417). C.D.S. received salary support from R01 AI148471. NIH P30 AR048311 and P30 AI027767 provided support for the UAB Consolidated Flow Cytometry Core and NIH P30CA13148 provided support for the O'Neal Comprehensive Cancer Center Tissue Procurement Facility.

References

1. Andrews SF, Huang Y, Kaur K, Popova LI, Ho IY, Pauli NT, Henry Dunand CJ, Taylor WM, Lim S, Huang M, et al. (2015). Immune history profoundly affects broadly protective B cell responses to influenza. Sci Transl Med 7, 316ra192. 10.1126/scitranslmed.aad0522.
2. Turner JS, Zhou JQ, Han J, Schmitz AJ, Rizk AA, Alsoussi WB, Lei T, Amor M, McIntire KM, Meade P, et al. (2020). Human germinal centres engage memory and naive B cells after influenza vaccination. Nature 586, 127–132. 10.1038/s41586-020-2711-0. [PubMed: 32866963]
3. Lee FE, Halliley JL, Walsh EE, Moscatiello AP, Kmush BL, Falsey AR, Randall TD, Kaminiski DA, Miller RK, and Sanz I (2011). Circulating human antibody-secreting cells during vaccinations and respiratory viral infections are characterized by high specificity and lack of bystander effect. J Immunol 186, 5514–5521. 10.4049/jimmunol.1002932. [PubMed: 21441455]
4. Laidlaw BJ, and Cyster JG (2020). Transcriptional regulation of memory B cell differentiation. Nat Rev Immunol. 10.1038/s41577-020-00446-2.
5. Yao C, Lou G, Sun HW, Zhu Z, Sun Y, Chen Z, Chauss D, Moseman EA, Cheng J, D'Antonio MA, et al. (2021). BACH2 enforces the transcriptional and epigenetic programs of stem-like CD8(+) T cells. Nat Immunol. 10.1038/s41590-021-00868-7.
6. Pais Ferreira D, Silva JG, Wyss T, Fuertes Marraco SA, Scarpellino L, Charmoy M, Maas R, Siddiqui I, Tang L, Joyce JA, et al. (2020). Central memory CD8(+) T cells derive from stem-like Tcf7(hi) effector cells in the absence of cytotoxic differentiation. Immunity 53, 985–1000 e1011. 10.1016/j.immuni.2020.09.005. [PubMed: 33128876]
7. Kurachi M, Barnitz RA, Yosef N, Odorizzi PM, DiIorio MA, Lemieux ME, Yates K, Godec J, Klatt MG, Regev A, et al. (2014). The transcription factor BATF operates as an essential differentiation checkpoint in early effector CD8+ T cells. Nat Immunol 15, 373–383. 10.1038/ni.2834. [PubMed: 24584090]

8. Kallies A, and Good-Jacobson KL (2017). Transcription Factor T-bet Orchestrates Lineage Development and Function in the Immune System. Trends Immunol 38, 287–297. 10.1016/j.it.2017.02.003. [PubMed: 28279590]
9. Shinnakasu R, Inoue T, Kometani K, Moriyama S, Adachi Y, Nakayama M, Takahashi Y, Fukuyama H, Okada T, and Kurosaki T (2016). Regulated selection of germinal-center cells into the memory B cell compartment. Nat Immunol 17, 861–869. 10.1038/ni.3460. [PubMed: 27158841]
10. Kometani K, Nakagawa R, Shinnakasu R, Kaji T, Rybouchkin A, Moriyama S, Furukawa K, Koseki H, Takemori T, and Kurosaki T (2013). Repression of the transcription factor Bach2 contributes to predisposition of IgG1 memory B cells toward plasma cell differentiation. Immunity 39, 136–147. 10.1016/j.immuni.2013.06.011. [PubMed: 23850379]
11. Igarashi K, Ochiai K, Itoh-Nakadai A, and Muto A (2014). Orchestration of plasma cell differentiation by Bach2 and its gene regulatory network. Immunol Rev 261, 116–125. 10.1111/imr.12201. [PubMed: 25123280]
12. Stone SL, Peel JN, Scharer CD, Risley CA, Chisolm DA, Schultz MD, Yu B, Ballesteros-Tato A, Wojciechowski W, Mousseau B, et al. (2019). T-bet Transcription Factor Promotes Antibody-Secreting Cell Differentiation by Limiting the Inflammatory Effects of IFN-gamma on B Cells. Immunity. 10.1016/j.immuni.2019.04.004.
13. Andrews SF, Chambers MJ, Schramm CA, Plyler J, Raab JE, Kanekiyo M, Gillespie RA, Ransier A, Darko S, Hu J, et al. (2019). Activation Dynamics and Immunoglobulin Evolution of Pre-existing and Newly Generated Human Memory B cell Responses to Influenza Hemagglutinin. Immunity 51, 398–410 e395. 10.1016/j.immuni.2019.06.024. [PubMed: 31350180]
14. Lau D, Lan LY, Andrews SF, Henry C, Rojas KT, Neu KE, Huang M, Huang Y, DeKosky B, Palm AE, et al. (2017). Low CD21 expression defines a population of recent germinal center graduates primed for plasma cell differentiation. Sci Immunol 2. 10.1126/sciimmunol.aai8153.
15. Ellebedy AH, Jackson KJ, Kissick HT, Nakaya HI, Davis CW, Roskin KM, McElroy AK, Oshansky CM, Elbein R, Thomas S, et al. (2016). Defining antigen-specific plasmablast and memory B cell subsets in human blood after viral infection or vaccination. Nat Immunol 17, 1226–1234. 10.1038/ni.3533. [PubMed: 27525369]
16. Tipton CM, Fucile CF, Darce J, Chida A, Ichikawa T, Gregoretti I, Schieferl S, Hom J, Jenks S, Feldman RJ, et al. (2015). Diversity, cellular origin and autoreactivity of antibody-secreting cell population expansions in acute systemic lupus erythematosus. Nat Immunol 16, 755–765. 10.1038/ni.3175. [PubMed: 26006014]
17. Oestreich KJ, and Weinmann AS (2012). T-bet employs diverse regulatory mechanisms to repress transcription. Trends Immunol 33, 78–83. 10.1016/j.it.2011.10.005. [PubMed: 22133865]
18. Shaffer AL, Emre NC, Lamy L, Ngo VN, Wright G, Xiao W, Powell J, Dave S, Yu X, Zhao H, et al. (2008). IRF4 addiction in multiple myeloma. Nature 454, 226–231. 10.1038/nature07064. [PubMed: 18568025]
19. Yu B, Zhang K, Milner JJ, Toma C, Chen R, Scott-Browne JP, Pereira RM, Crotty S, Chang JT, Pipkin ME, et al. (2017). Epigenetic landscapes reveal transcription factors that regulate CD8(+) T cell differentiation. Nat Immunol 18, 573–582. 10.1038/ni.3706. [PubMed: 28288100]
20. Lazarevic V, Glimcher LH, and Lord GM (2013). T-bet: a bridge between innate and adaptive immunity. Nat Rev Immunol 13, 777–789. 10.1038/nri3536. [PubMed: 24113868]
21. Omilusik KD, and Goldrath AW (2019). Remembering to remember: T cell memory maintenance and plasticity. Curr Opin Immunol 58, 89–97. 10.1016/j.coi.2019.04.009. [PubMed: 31170601]
22. Kaech SM, Hemby S, Kersh E, and Ahmed R (2002). Molecular and functional profiling of memory CD8 T cell differentiation. Cell 111, 837–851. 10.1016/s0092-8674(02)01139-x. [PubMed: 12526810]
23. Luckey CJ, Bhattacharya D, Goldrath AW, Weissman IL, Benoist C, and Mathis D (2006). Memory T and memory B cells share a transcriptional program of self-renewal with long-term hematopoietic stem cells. Proc Natl Acad Sci U S A 103, 3304–3309. 10.1073/pnas.0511137103. [PubMed: 16492737]
24. Zhou X, and Xue HH (2012). Cutting edge: generation of memory precursors and functional memory CD8+ T cells depends on T cell factor-1 and lymphoid enhancer-binding factor-1. J Immunol 189, 2722–2726. 10.4049/jimmunol.1201150. [PubMed: 22875805]

25. Consortium EP (2012). An integrated encyclopedia of DNA elements in the human genome. Nature 489, 57–74. 10.1038/nature11247. [PubMed: 22955616]
26. Liberzon A, Subramanian A, Pinchback R, Thorvaldsdottir H, Tamayo P, and Mesirov JP (2011). Molecular signatures database (MSigDB) 3.0. Bioinformatics 27, 1739–1740. 10.1093/bioinformatics/btr260. [PubMed: 21546393]
27. Bertolotti M, Sitia R, and Rubartelli A (2012). On the redox control of B lymphocyte differentiation and function. Antioxid Redox Signal 16, 1139–1149. 10.1089/ars.2011.4252. [PubMed: 22229488]
28. Oikonomou C, and Hendershot LM (2020). Disposing of misfolded ER proteins: A troubled substrate's way out of the ER. Mol Cell Endocrinol 500, 110630. 10.1016/j.mce.2019.110630. [PubMed: 31669350]
29. Li H, Borrego F, Nagata S, and Tolnay M (2016). Fc Receptor-like 5 Expression Distinguishes Two Distinct Subsets of Human Circulating Tissue-like Memory B Cells. J Immunol 196, 4064–4074. 10.4049/jimmunol.1501027. [PubMed: 27076679]
30. van Anken E, Romijn EP, Maggioni C, Mezghrani A, Sitia R, Braakman I, and Heck AJ (2003). Sequential waves of functionally related proteins are expressed when B cells prepare for antibody secretion. Immunity 18, 243–253. 10.1016/s1074-7613(03)00024-4. [PubMed: 12594951]
31. Price MJ, Patterson DG, Scharer CD, and Boss JM (2018). Progressive Upregulation of Oxidative Metabolism Facilitates Plasmablast Differentiation to a T-Independent Antigen. Cell Rep 23, 3152–3159. 10.1016/j.celrep.2018.05.053. [PubMed: 29898388]
32. Benhamron S, Pattanayak SP, Berger M, and Tirosh B (2015). mTOR activation promotes plasma cell differentiation and bypasses XBP-1 for immunoglobulin secretion. Mol Cell Biol 35, 153–166. 10.1128/MCB.01187-14. [PubMed: 25332234]
33. Pengo N, Scolari M, Oliva L, Milan E, Mainoldi F, Raimondi A, Fagioli C, Merlini A, Mariani E, Pasqualetto E, et al. (2013). Plasma cells require autophagy for sustainable immunoglobulin production. Nat Immunol 14, 298–305. 10.1038/ni.2524. [PubMed: 23354484]
34. Jenks SA, Cashman KS, Zumaquero E, Marigorta UM, Patel AV, Wang X, Tomar D, Woodruff MC, Simon Z, Bugrovsky R, et al. (2018). Distinct Effector B Cells Induced by Unregulated Toll-like Receptor 7 Contribute to Pathogenic Responses in Systemic Lupus Erythematosus. Immunity 49, 725–739 e726. 10.1016/j.immuni.2018.08.015. [PubMed: 30314758]
35. Gaudette BT, Jones DD, Bortnick A, Argon Y, and Allman D (2020). mTORC1 coordinates an immediate unfolded protein response-related transcriptome in activated B cells preceding antibody secretion. Nat Commun 11, 723. 10.1038/s41467-019-14032-1. [PubMed: 32024827]
36. Woodland DL, and Kohlmeier JE (2009). Migration, maintenance and recall of memory T cells in peripheral tissues. Nat Rev Immunol 9, 153–161. 10.1038/nri2496. [PubMed: 19240755]
37. Wrammert J, Smith K, Miller J, Langley WA, Kokko K, Larsen C, Zheng NY, Mays I, Garman L, Helms C, et al. (2008). Rapid cloning of high-affinity human monoclonal antibodies against influenza virus. Nature 453, 667–671. 10.1038/nature06890. [PubMed: 18449194]
38. Kim CC, Baccarella AM, Bayat A, Pepper M, and Fontana MF (2019). FCRL5(+) Memory B Cells Exhibit Robust Recall Responses. Cell Rep 27, 1446–1460 e1444. 10.1016/j.celrep.2019.04.019. [PubMed: 31042472]
39. Buck MD, Sowell RT, Kaech SM, and Pearce EL (2017). Metabolic Instruction of Immunity. Cell 169, 570–586. 10.1016/j.cell.2017.04.004. [PubMed: 28475890]
40. Lam WY, Jash A, Yao CH, D'Souza L, Wong R, Nunley RM, Meares GP, Patti GJ, and Bhattacharya D (2018). Metabolic and Transcriptional Modules Independently Diversify Plasma Cell Lifespan and Function. Cell Rep 24, 2479–2492 e2476. 10.1016/j.celrep.2018.07.084. [PubMed: 30157439]
41. Lam WY, and Bhattacharya D (2018). Metabolic Links between Plasma Cell Survival, Secretion, and Stress. Trends Immunol 39, 19–27. 10.1016/j.it.2017.08.007. [PubMed: 28919256]
42. Ma Y, Shimizu Y, Mann MJ, Jin Y, and Hendershot LM (2010). Plasma cell differentiation initiates a limited ER stress response by specifically suppressing the PERK-dependent branch of the unfolded protein response. Cell Stress Chaperones 15, 281–293. 10.1007/s12192-009-0142-9. [PubMed: 19898960]

43. Xu W, Zhao X, Wang X, Feng H, Gou M, Jin W, Wang X, Liu X, and Dong C (2019). The Transcription Factor Tox2 Drives T Follicular Helper Cell Development via Regulating Chromatin Accessibility. Immunity 51, 826–839 e825. 10.1016/j.immuni.2019.10.006. [PubMed: 31732165]
44. Lin D, Ippolito GC, Zong RT, Bryant J, Koslovsky J, and Tucker P (2007). Bright/ARID3A contributes to chromatin accessibility of the immunoglobulin heavy chain enhancer. Mol Cancer 6, 23. 10.1186/1476-4598-6-23. [PubMed: 17386101]
45. Bentebibel SE, Lopez S, Obermoser G, Schmitt N, Mueller C, Harrod C, Flano E, Mejias A, Albrecht RA, Blankenship D, et al. (2013). Induction of ICOS+CXCR3+CXCR5+ TH cells correlates with antibody responses to influenza vaccination. Sci Transl Med 5, 176ra132. 10.1126/scitranslmed.3005191.
46. Nakaya HI, Hagan T, Duraisingham SS, Lee EK, Kwissa M, Rouphael N, Frasca D, Gersten M, Mehta AK, Gaujoux R, et al. (2015). Systems Analysis of Immunity to Influenza Vaccination across Multiple Years and in Diverse Populations Reveals Shared Molecular Signatures. Immunity 43, 1186–1198. 10.1016/j.immuni.2015.11.012. [PubMed: 26682988]
47. Hafemeister C, and Satija R (2019). Normalization and variance stabilization of single-cell RNA-seq data using regularized negative binomial regression. Genome Biol 20, 296. 10.1186/s13059-019-1874-1. [PubMed: 31870423]
48. Scharer CD, Blalock EL, Mi T, Barwick BG, Jenks SA, Deguchi T, Cashman KS, Neary BE, Patterson DG, Hicks SL, et al. (2019). Epigenetic programming underpins B cell dysfunction in human SLE. Nat Immunol 20, 1071–1082. 10.1038/s41590-019-0419-9. [PubMed: 31263277]
49. Hipp N, Symington H, Pastoret C, Caron G, Monvoisin C, Tarte K, Fest T, and Delaloy C (2017). IL-2 imprints human naive B cell fate towards plasma cell through ERK/ELK1-mediated BACH2 repression. Nat Commun 8, 1443. 10.1038/s41467-017-01475-7. [PubMed: 29129929]
50. Alamyar E, Duroux P, Lefranc MP, and Giudicelli V (2012). IMGT((R)) tools for the nucleotide analysis of immunoglobulin (IG) and T cell receptor (TR) V-(D)-J repertoires, polymorphisms, and IG mutations: IMGT/V-QUEST and IMGT/HighV-QUEST for NGS. Methods Mol Biol 882, 569–604. 10.1007/978-1-61779-842-9_32. [PubMed: 22665256]
51. Dobin A, Davis CA, Schlesinger F, Drenkow J, Zaleski C, Jha S, Batut P, Chaisson M, and Gingeras TR (2013). STAR: ultrafast universal RNA-seq aligner. Bioinformatics 29, 15–21. 10.1093/bioinformatics/bts635. [PubMed: 23104886]
52. Lawrence M, Huber W, Pages H, Aboyoun P, Carlson M, Gentleman R, Morgan MT, and Carey VJ (2013). Software for computing and annotating genomic ranges. PLoS Comput Biol 9, e1003118. 10.1371/journal.pcbi.1003118. [PubMed: 23950696]
53. Robinson MD, McCarthy DJ, and Smyth GK (2010). edgeR: a Bioconductor package for differential expression analysis of digital gene expression data. Bioinformatics 26, 139–140. 10.1093/bioinformatics/btp616. [PubMed: 19910308]
54. Benjamini Y, and Hochberg Y (1995). Controlling the fase discovery rate: a practical and powerful approach to multiple testing. Journal of the Royal statistical society: series B (Methodological) 57, 289–300.
55. Subramanian A, Tamayo P, Mootha VK, Mukherjee S, Ebert BL, Gillette MA, Paulovich A, Pomeroy SL, Golub TR, Lander ES, and Mesirov JP (2005). Gene set enrichment analysis: a knowledge-based approach for interpreting genome-wide expression profiles. Proc Natl Acad Sci U S A 102, 15545–15550. 10.1073/pnas.0506580102. [PubMed: 16199517]
56. Tibshirani R WG, Hastie T (2001). Estimating the number of clusters in a data set via the gap statistic. Journal of the Royal statistical society: series B (Methodological) 63, 411–423.
57. Langmead B (2010). Aligning short sequencing reads with Bowtie. Curr Protoc Bioinformatics Chapter 11, Unit 11 17. 10.1002/0471250953.bi1107s32.
58. Zhang Y, Liu T, Meyer CA, Eeckhoute J, Johnson DS, Bernstein BE, Nusbaum C, Myers RM, Brown M, Li W, and Liu XS (2008). Model-based analysis of ChIP-Seq (MACS). Genome Biol 9, R137. 10.1186/gb-2008-9-9-r137. [PubMed: 18798982]
59. Heinz S, Benner C, Spann N, Bertolino E, Lin YC, Laslo P, Cheng JX, Murre C, Singh H, and Glass CK (2010). Simple combinations of lineage-determining transcription factors prime cis-regulatory elements required for macrophage and B cell identities. Mol Cell 38, 576–589. 10.1016/j.molcel.2010.05.004. [PubMed: 20513432]

60. Scharer CD, Blalock EL, Barwick BG, Haines RR, Wei C, Sanz I, and Boss JM (2016). ATAC-seq on biobanked specimens defines a unique chromatin accessibility structure in naive SLE B cells. Sci Rep 6, 27030. 10.1038/srep27030. [PubMed: 27249108]

61. Butler A, Hoffman P, Smibert P, Papalexi E, and Satija R (2018). Integrating single-cell transcriptomic data across different conditions, technologies, and species. Nat Biotechnol 36, 411–420. 10.1038/nbt.4096. [PubMed: 29608179]

62. Allie SR, Bradley JE, Mudunuru U, Schultz MD, Graf BA, Lund FE, and Randall TD (2019). The establishment of resident memory B cells in the lung requires local antigen encounter. Nat Immunol 20, 97–108. 10.1038/s41590-018-0260-6. [PubMed: 30510223]

Highlights

- FcRL5^{+}T-bet^{+} memory B cells are molecularly programmed for effector function
- FcRL5^{+} T-bet^{+} memory B cells are metabolically poised to form antibody-secreting cells
- FcRL5^{+} T-bet^{+} memory B cells predict long-lived antibody responses to flu vaccination

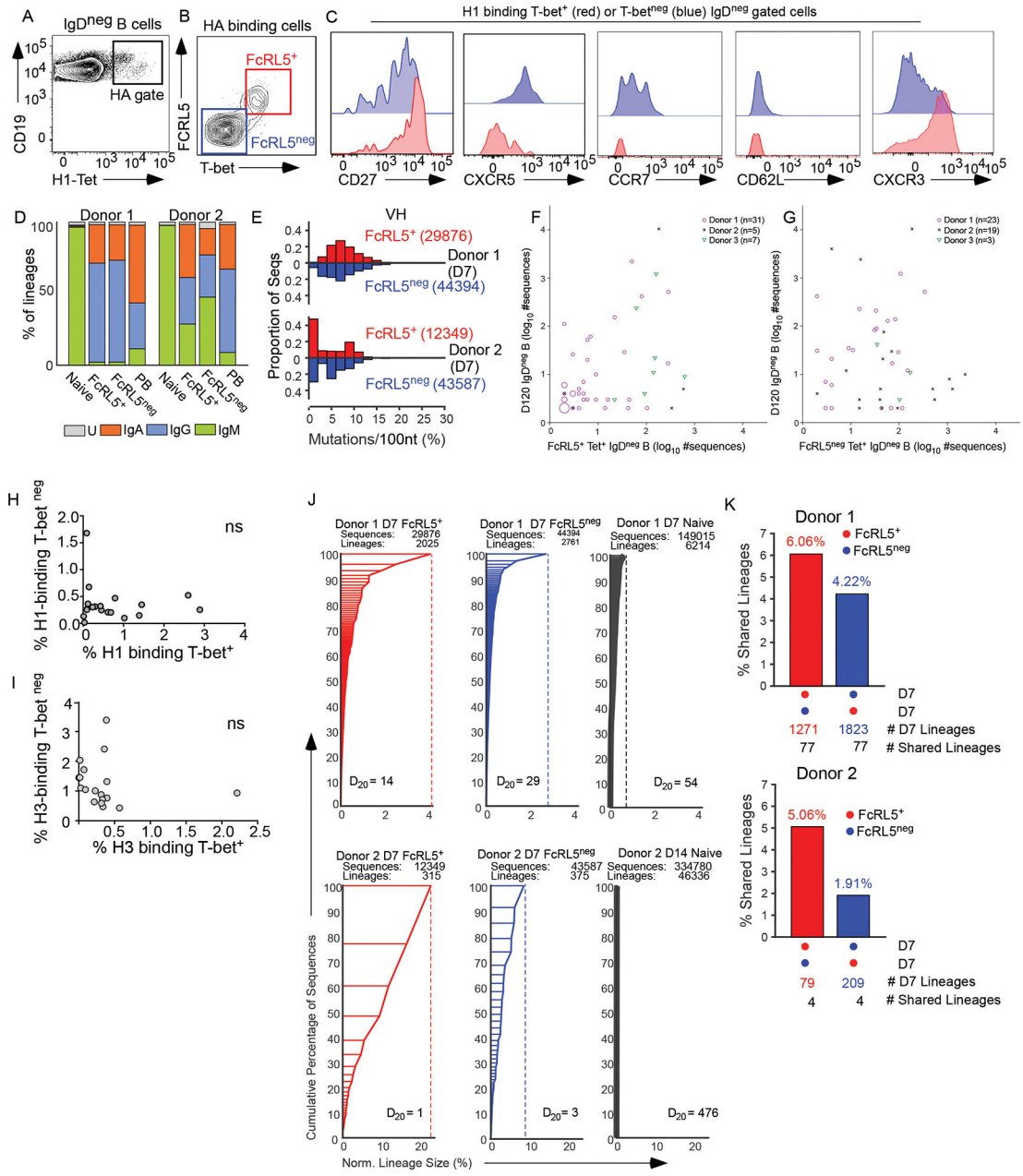

Figure 1. Seasonal influenza vaccination elicits distinct HA-specific Bmem cell subsets.

(**A-C**) FACS plots showing HA-tetramer binding versus CD19 expression (**A**) and FcRL5 versus T-bet expression (**B**) by HA-specific IgD^{neg} B cells from blood of a D7 post-IIV HD. Histograms (**C**) showing cell surface marker expression by the H1-specific IgD^{neg} T-bet^{+} (red) and T-bet^{neg} (blue) B cells.

(**D-E**) IGH V_H BCR repertoire analysis of sort-purified circulating H3-specific FcRL5^{+} and FcRL5^{neg} IgD^{neg} B cells, IgD^{+} naïve B cells, and IgD^{neg}CD38^{hi} PBs from 2 HD on D7 post-IIV. Isotype distribution (**D**) in each D7 subset (U = "unidentified"). Distribution of V_H sequence mutation frequencies (**E**) in H3-specific IgD^{neg} FcRL5^{+} and FcRL5^{neg} cells. Number of sequences in each population indicated.

(**F-G**) Shared lineages between D120 total IgD^{neg} B cells (y-axis) and HA-specific $FcRL5^{+}$ (**F**) or $FcRL5^{neg}$ (**G**) IgD^{neg} B cells (x-axis) from 3 HDs on D7 or D14 post-IIV. Axes indicate size of shared lineages (symbols) defined as ≥2 sequences in each lineage in each population. Numbers of shared lineages (n) for each donor indicated. Larger symbols represent multiple shared lineages of the same sizes.

(**H-I**) Frequencies of T-bet^{+} and T-bet^{neg} cells within H1-specific (**H**) or H3-specific (**I**) IgD^{neg} B cell subsets measured in each individual (n=19) on D7 post-IIV. ns = not significant.

(**J**) V_H BCR lineages in sort-purified naïve and D7 H3-specific $FcRL5^{+}$ or $FcRL5^{neg}$ IgD^{neg} B cells with lineages ordered by size (y-axis) and % of total number of sequences (x-axis). Data reported as Diversity index 20 (D_{20}) values, total number of sequences per subset, and lineages per subset.

(**K**) Lineage sharing between D7 $FcRL5^{+}$ and $FcRL5^{neg}$ subsets reported as percentage of shared non-singleton lineages. The numbers of shared and total non-singleton lineages per donor and subset also reported.

Additional BCR repertoire data reported in Table S1, Fig 1F–J and Fig. S1N. See Fig. S1 for gating strategy and additional phenotypic characterization of B cell subsets.

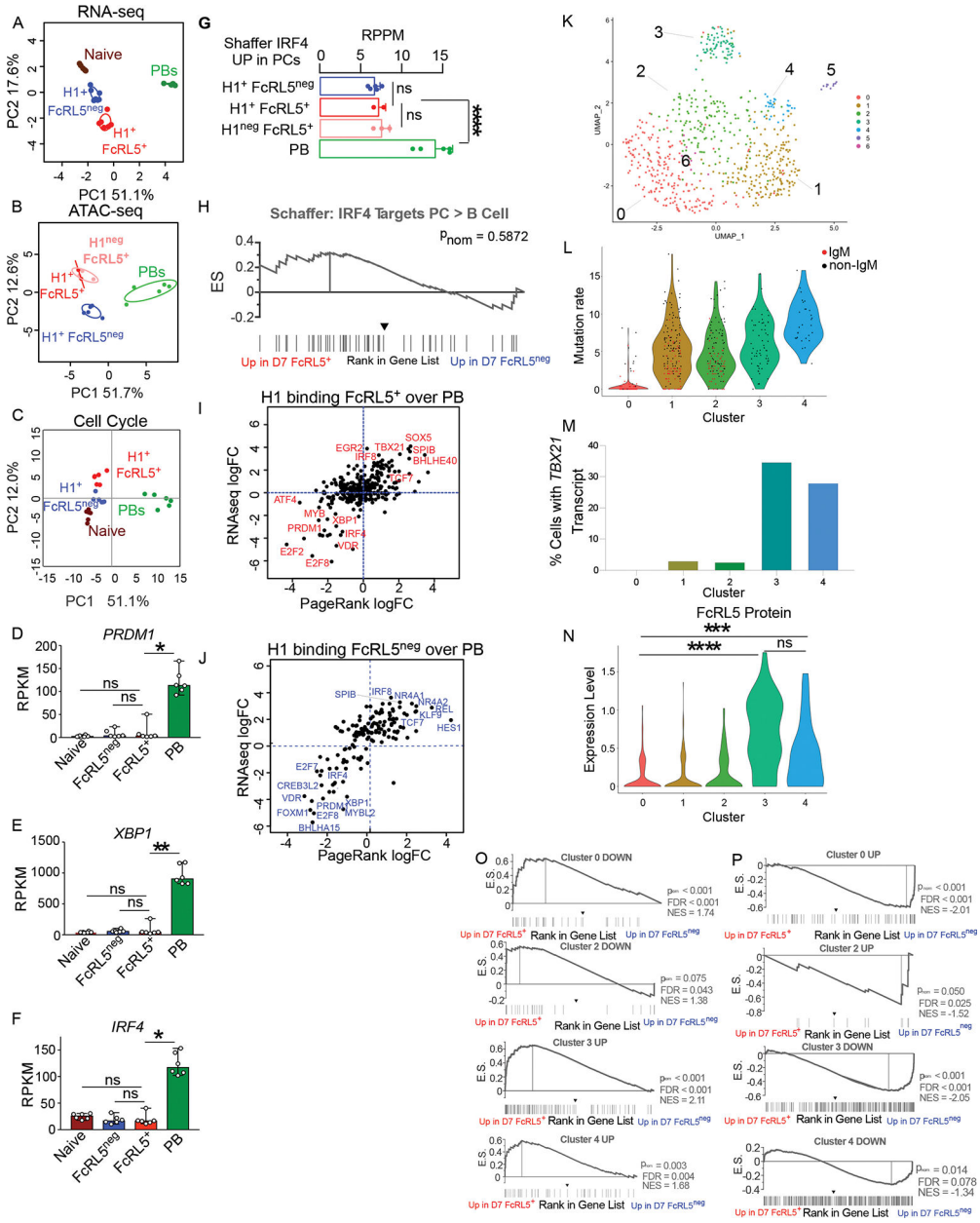

Figure 2. H1-specific FcRL5^{+} and FcRL5^{neg} Bmem cells are transcriptionally and epigenetically distinct.

(**A-J**) RNA-seq and ATAC-seq analyses performed on D7 post-IIV B lineage subsets from 5–6 HDs.

(**A-B**) PCA of RNA-seq (**A**) and ATAC-seq (**B**) data sets from D7 B lineage subsets.

(**C**) PCA of cell cycle genes expressed by D7 B cell subsets.

(**D-F**) *PRDM1* (**D**), *XBP1* (**E**) and *IRF4* (**F**) mRNA expression by D7 B cell subsets.

(**G-H**) Accessibility and expression of published[18] IRF4-regulated ASC genes by D7 B lineage subsets. Chromatin accessibility surrounding IRF4 ASC regulon genes (**G**) is reported as the mean peak accessibility for all peaks mapping to IRF4 ASC regulon genes.

GSEA (**H**) comparing the RNA-seq ranked gene list from D7 H1-specific IgD^{neg} FcRL5^{+} vs FcRL5^{neg} B cells to the IRF4 ASC regulon gene set.

(**I-J**) PR identified TFs predicted to regulate gene networks in D7 PBs and IgD^{neg} H1-specific Bmem cell subsets. Data reported as logFC in PR score and logFC in mRNA expression of each TF with D7 FcRL5^{+} Bmem cells over PB (**I**) or D7 FcRL5^{neg} Bmem cells over PBs (**J**). Selected TFs indicated.

(**K-P**) Single cell RNA-seq, BCR-seq and CITE-seq analyses of sort-purified HA-specific IgD^{neg} B cells from 2 HD between D7-D21 post-IIV.

(**K**) UMAP showing transcriptional clusters (C0-C6) from single cell RNA-seq data.

(**L**) BCR-seq analysis of single cells in Clusters C0-C4. Data reported as V_H gene mutation frequency. Unswitched (IgM^{+}, red dots) and switched (black dots) cells are shown.

(**M**) *TBX21* expression reported as % of cells in each cluster with at least one *TBX21* transcript.

(**N**) CITE-seq analysis of FcRL5 protein in HA-specific IgD^{neg} in Clusters C0-C4. Expression in single cells normalized using scTransform[47] and shown as violin plots.

(**O-P**) GSEA comparing the ranked gene list from D7 H1-specific IgD^{neg} FcRL5^{+} vs FcRL5^{neg} B cells to the upregulated or downregulated DEGs in each single cell cluster. Data shown include single cell DEG sets enriched in D7 H1-specific IgD^{neg} FcRL5^{+} (**O**) or FcRL5^{neg} (**P**) B cells. p_{nom} values indicated.

Data sets for RNA-seq, ATAC-seq, PR analysis, GSEA gene sets, and sc-seq datasets are provided in Tables S2–S4. Fig. S2 has additional RNA expression analysis from D7 (S2A-B) and D14 (S2C-I) B lineage subsets. Statistical analyses performed using one-way ANOVA (**D-F, N**). *p< 0.05, **, p<0.01, *** p<0.001, **** p <0.0001 ns= non-significant.

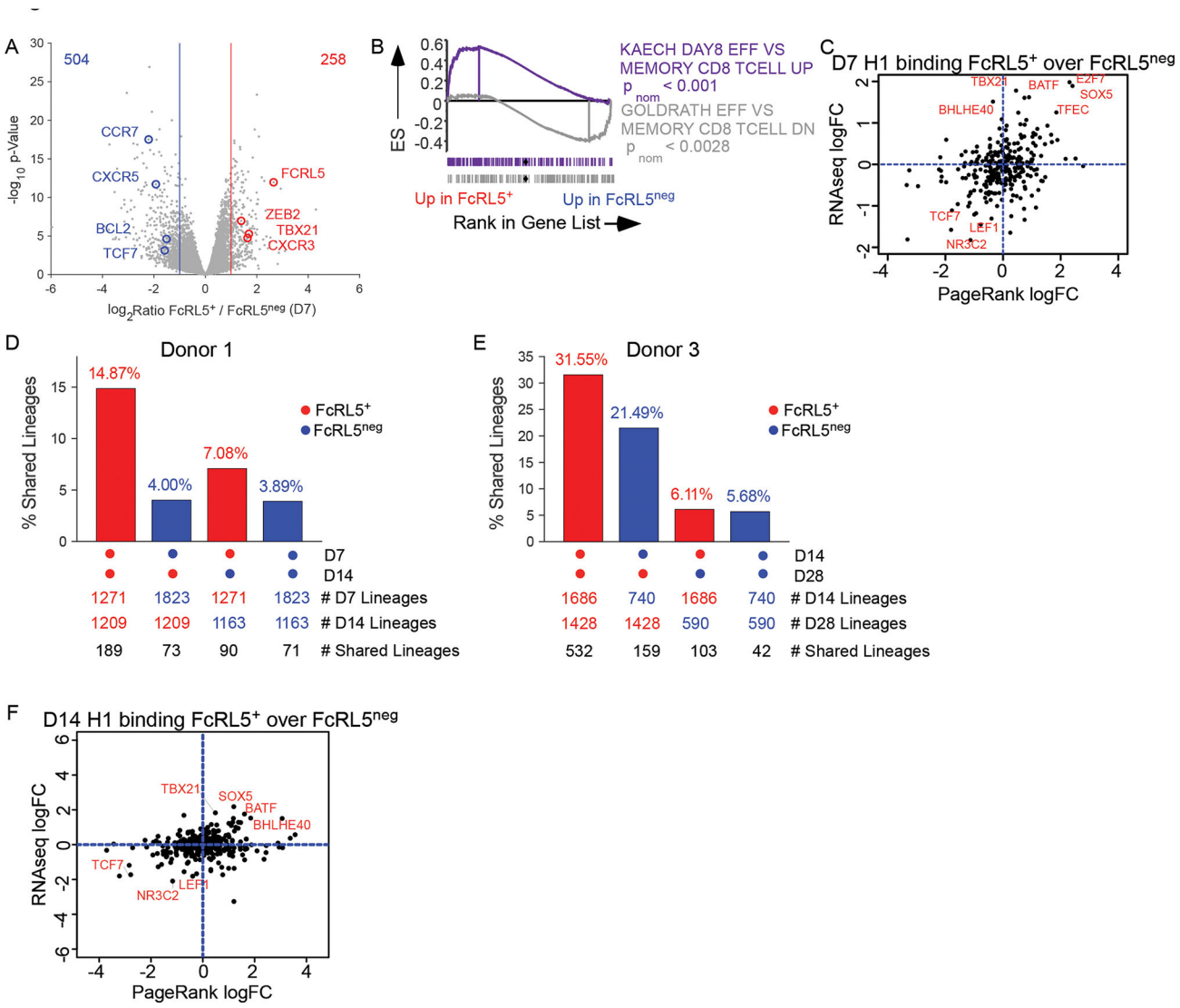

Figure 3. Division of H1-specific B cells into FcRL5^{+} effector-like and FcRL5^{neg} stem-like Bmem cells.

(A) Volcano plot showing DEG upregulated in D7 H1-specific IgD^{neg} FcRL5^{+} (red) and FcRL5^{neg} (blue) Bmem cells.

(B) GSEA comparing the ranked gene list from D7 H1-specific IgD^{neg} FcRL5^{+} and FcRL5^{neg} B cells to DEG that are either upregulated (KAECH[22]) or down-regulated (GOLDRATH[23]) in effector vs memory CD8^{+} T cells.

(C) TFs identified by PR as regulators of the D7 H1-specific IgD^{neg} FcRL5^{+} and D7 H1-specific IgD^{neg} FcRL5^{neg} gene networks.

(**D-E**) Shared BCR V_H lineages between H1-specific IgD^{neg} Bmem cells isolated from the same donor at sequential timepoints. Data reported as percentage of shared lineages between different Bmem cell populations over time. The numbers of non-singleton lineages identified in each subset at each timepoint and the numbers of shared lineages for each pairwise comparison indicated.

(F) TFs identified by PR as regulators of D14 H1-specific IgD^{neg} $FcRL5^{+}$ and D14 H1-specific IgD^{neg} $FcRL5^{neg}$ gene networks.

Data sets for BCR repertoire, RNA-seq, PR, and GSEA genesets provided in Tables S1–S3.

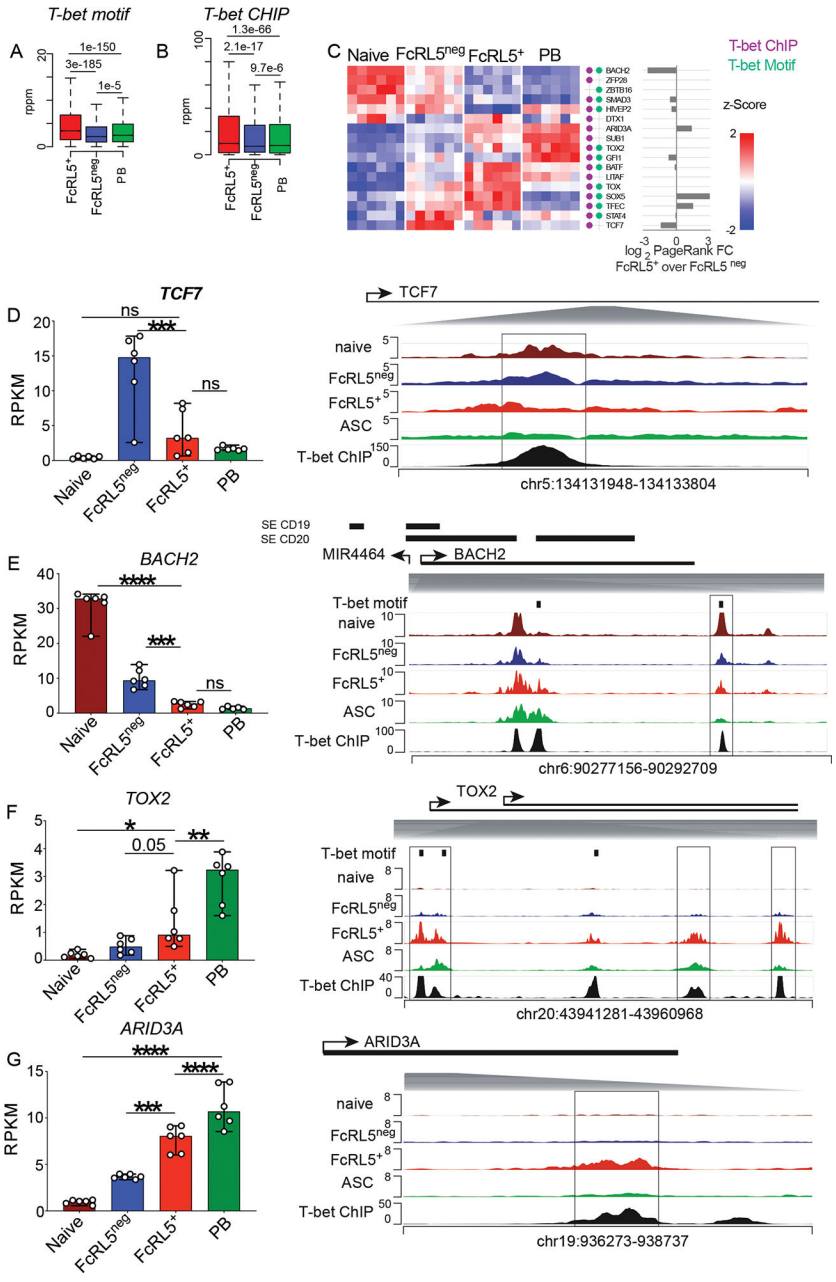

Figure 4. The transcriptome and epigenome of FcRL5^{+} Bmem cells display T-bet associated changes.

(**A-B**) Box plots showing chromatin accessibility surrounding (within 50 bp) defined T-bet motifs (**A**) and previously identified T-bet ChIP-seq peaks[25] (**B**) in memory FcRL5^{+}, FcRL5^{neg} and PB populations.

(**C**) Expression of transcriptional regulators (n=17) that were identified as DEG between FcRL5^{+} and FcRL5^{neg} Bmem cells and were also assigned to at least one DAR that contained a T-bet binding motif (green dots) and/or ChIP-seq T-bet binding site[25] (purple dot). Data shown as a heat map displaying per-regulator gene z-scores of log expression in the indicated subsets. PR scores for each regulator shown as absolute value $\log_2$ FC of FcRL5^{+} over FcRL5^{neg} cells.

(**D**-**G**) RNA-seq expression and genome ATAC-seq plots for *TCF7* (**D**), *BACH2* (**E**), *TOX2* (**F**) and *ARID3A* (**G**). Genome ATAC-seq plots aligned with ChIP-seq T-bet binding sites[25] and with ATAC-seq from resting naïve B cells[48]. Boxes indicate loci with significant DAR. Vertical black bars indicate HOMER-predicted consensus T-bet binding motifs. Super-enhancers in *BACH2* locus identified in $CD19^+$ and $CD20^+$ human B cells[49] shown as horizontal black bars. Shaded gray triangles indicate location of DAR-containing regions within each locus. Statistical analyses were performed using one-way ANOVA (**D**-**G**). *p< 0.05, **, p<0.01, *** p<0.001, **** p <0.0001 ns= non-significant.

Data sets for RNA-seq, ATAC-seq, transcriptional regulators and PR analyses are provided in Tables S2–S3.

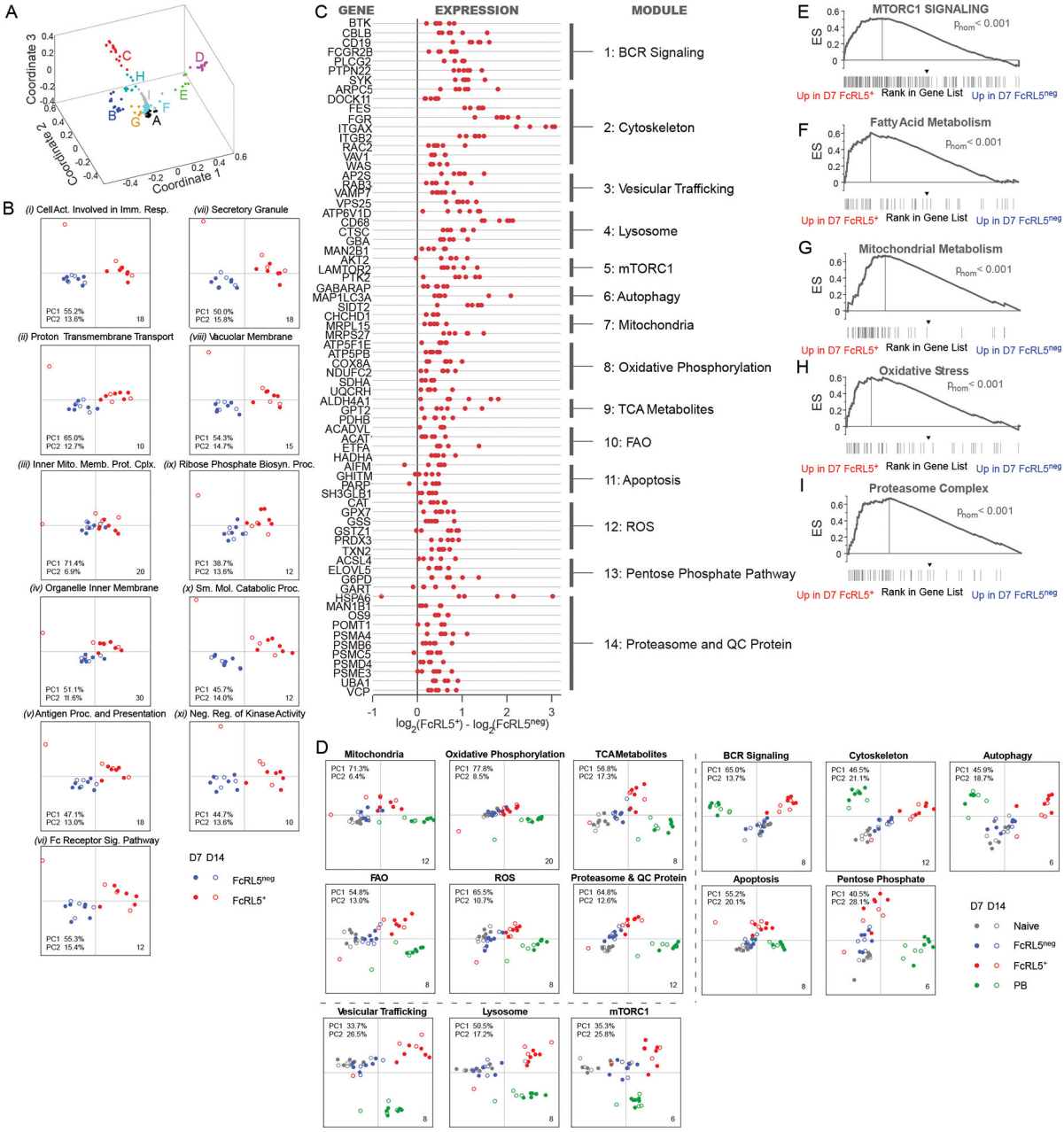

Figure 5. Metabolic gene expression differs between FcRL5^{+} effector and FcRL5^{neg} stem-like Bmem cells.

(**A-C**) Identification of signaling and metabolic gene modules in FcRL5^{+} Bmem cells. Clustering (**A**) of leading-edge genes from 185 GO gene lists (mSigDB v.7) that were enriched (FDR q < 0.01) for expression in D7 FcRL5^{+} relative to D7 FcRL5^{neg} Bmem cells. Nine clusters (A-I) with overlapping leading edge gene sets were identified. Eleven prototypic GO gene lists (lists *i-xi*) representing the 9 GO gene set clusters were selected and the leading-edge genes from gene lists were functionally annotated and used for PCA (**B**) comparing D7 and D14 H1-specific IgD^{neg} FcRL5^{+} and FcRL5^{neg} Bmem cells. The leading-edge genes were grouped into 14 signaling and metabolic modules (**C**) with representative genes from each module shown as the difference in $\log_2$ FC in expression

by D7 H1-specific IgD^{neg} $FcRL5^{+}$ and $FcRL5^{neg}$ Bmem cells. Red dots indicate individual samples with FDR q<0.05. **(D)** PCA using the 14 module gene sets comparing naïve B, D7 PB and D7 or D14 H1-specific IgD^{neg} $FcRL5^{+}$ and $H1^{+}$ IgD^{neg} $FcRL5^{neg}$ Bmem cells. (**E-I**) GSEA comparing the RNA-seq ranked gene list from D7 H1-specific IgD^{neg} $FcRL5^{+}$ and $FcRL5^{neg}$ B cells to curated gene lists for mTORC1 signaling **(E)**, fatty acid metabolism **(F)**, mitochondrial metabolism **(G)**, oxidative stress **(H)** and proteasome complex **(I)**. GSEA p_{nom}-values indicated.

Table S2 and Fig. S3 include clustering and module data, leading-edge genes from prototypic GO-gene lists, and gene lists for the signaling and metabolism modules and GSEA genesets.

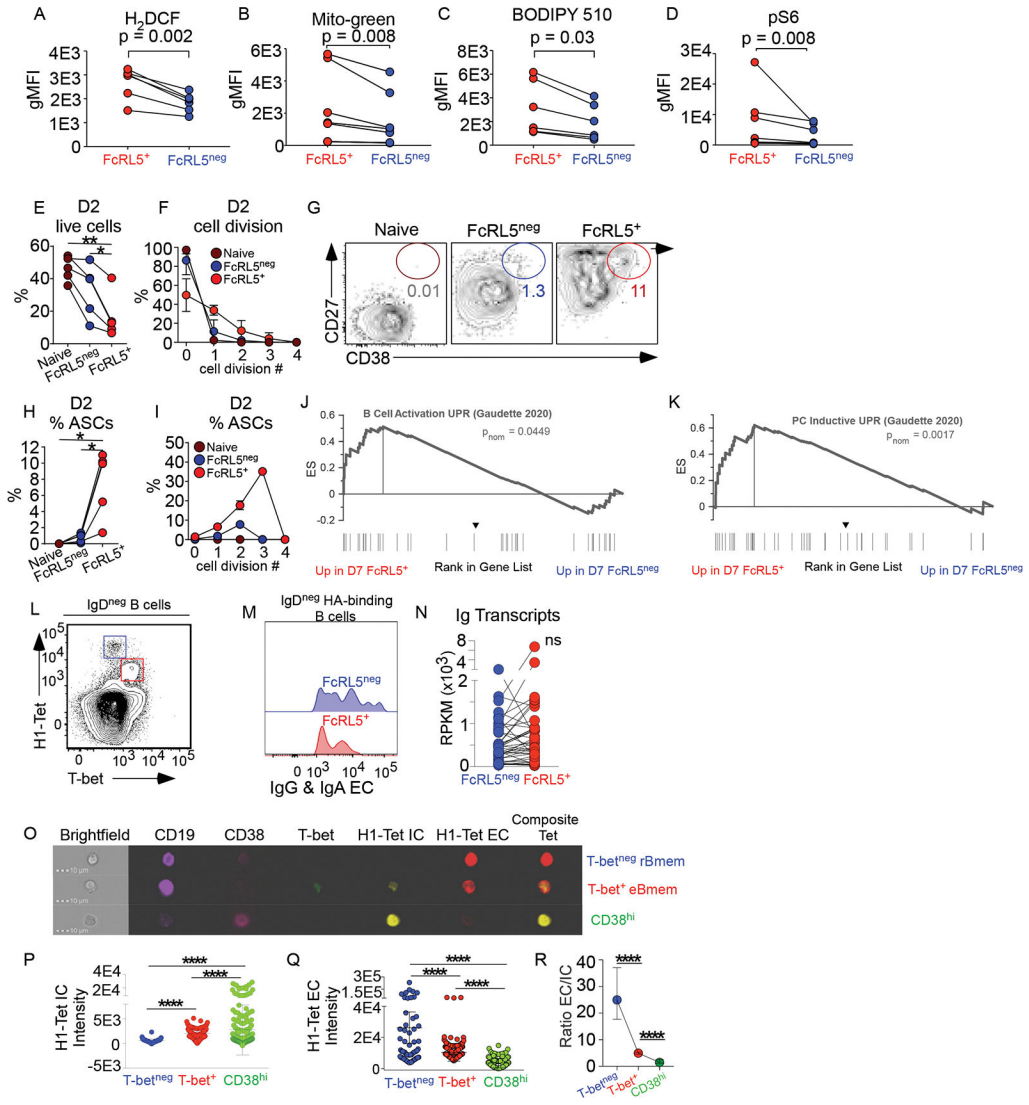

Figure 6. FcRL5^{+} Bmem cells are metabolically poised to secrete Ab.

(A-D) Metabolic flow assays using tonsil-derived matched (n=6–8 donors) FcRL5^{+} and FcRL5^{neg} IgD^{neg}CD27^{+} Bmem cells. ROS activity (**A**) measured with 2, 7–dichlorohydrofluorescein diacetate (H_2DCF). Mitochondrial mass (**B**) measured with Mitotracker Green. Membrane lipid composition **(C)** measured with BODIPY510. mTORC1 activation **(D)** measured with anti-phospho-S6 (pS6) kinase Ab. Data reported as geometric mean fluorescence (gMFI) and shown as paired analysis between FcRL5^{+} and FcRL5^{neg} cells purified from the same donor.

(**E-I**) Proliferation and differentiation of purified donor-matched naïve (brown), FcRL5^{+} (red) or FcrL5^{neg} (blue), IgD^{neg}CD27^{+}CD38$^{lo/med}$ tonsil Bmem cells. CTV labeled cells were stimulated with R848, IL-21, IL-2 and IFN-γ and assessed on D2. Cell survival (**E**) and frequency of cells per cell division (**F**) on D2 were determined by flow cytometry and reported as the mean ± SD (n = 5 donors). ASCs in D2 cultures enumerated by flow cytometry (**G**) with frequencies of total CD27^{hi}CD38^{hi} ASCs (**H**) and percentage of ASCs in each cell division (**I**) reported.

(J-K) GSEA comparing the ranked gene list from D7 H1-specific IgD^{neg} FcRL5^{+} and FcRL5^{neg} Bmem cells to genes[35] induced by the mTORC1-dependent B cell activation UPR (**J**) or the mTORC1-dependent PC inductive UPR (**K**).

(**L**) Flow cytometry showing H1 tetramer-binding by D7 T-bet^{+} and T-bet^{neg} IgD^{neg} gated B cells.

(**M**) Extracellular expression of IgG and IgA by D7 IgD^{neg} HA-specific FcRL5^{neg} and FcRL5^{+} Bmem cells after sequential staining with Abs to FcRL5, IgD, CD19 and HA tetramers (H1 and H3) followed by anti-IgG and anti-IgA Abs.

(**N**) RNA-seq analysis of IgH transcripts (*IgHG1, IgHG2, IgHG3, IgHG4, IgHA1, IgHA2)* from sort-purified D7 IgD^{neg} HA-specific FcRL5^{neg} and FcRL5^{+} Bmem cells.

(O-R) Image Stream analysis of sort-purified D7 post-IIV CD19^{+}IgD^{neg} cells measuring expression of CD38, plasma membrane Ig (detected with H1-APC tetramer), intracellular T-bet, and intracellular Ig (detected with H1-PE tetramer). Representative images (**O**) of individual CD38^{hi} PBs (n=211 cells), H1 tetramer-binding T-bet^{+} (n=195 cells) and T-bet^{neg} (n=62 cells) cells. Intensity of intracellular (IC) H1 tetramer staining **(P)** and extracellular (EC) H1 tetramer staining **(Q)** and the ratio of EC/IC H1 tetramer staining (**R**) in each T-bet^{neg}, T-bet^{+} and CD38^{hi} cell was determined. Ratio in (**R**) shown as median for the individual cells within each subset and error bars indicating the 95% confidence interval. Fig. S4 shows additional analyses of tonsil B cell subsets, gated or purified as in (Fig. S4A–C) and examined in metabolism assays (Fig. S4D–G) or after *in vitro* stimulation for 2–3 days (Fig. S4H–N). Table S2 and Fig. S5A provide mTORC1-controlled UPR gene set data. Table S5 and Fig. S5C–D report BCR affinity measurements. Fig. S5B shows HA-binding expression over 8 weeks post-IIV[2] and Fig. S5E shows expression of transmembrane and secretory Ig exon transcripts. Statistical analyses were performed using Wilcoxon matched-pairs signed rank tests (**A-D, N**), one-way ANOVA with Kruskal-Wallis Multiple Comparisons Testing (**P,Q**) and one-way ANOVA with Tukey's multiple comparison testing (**E, H, R**). *p< 0.05, **, p<0.01, *** p<0.001, **** p <0.0001 ns= non-significant.

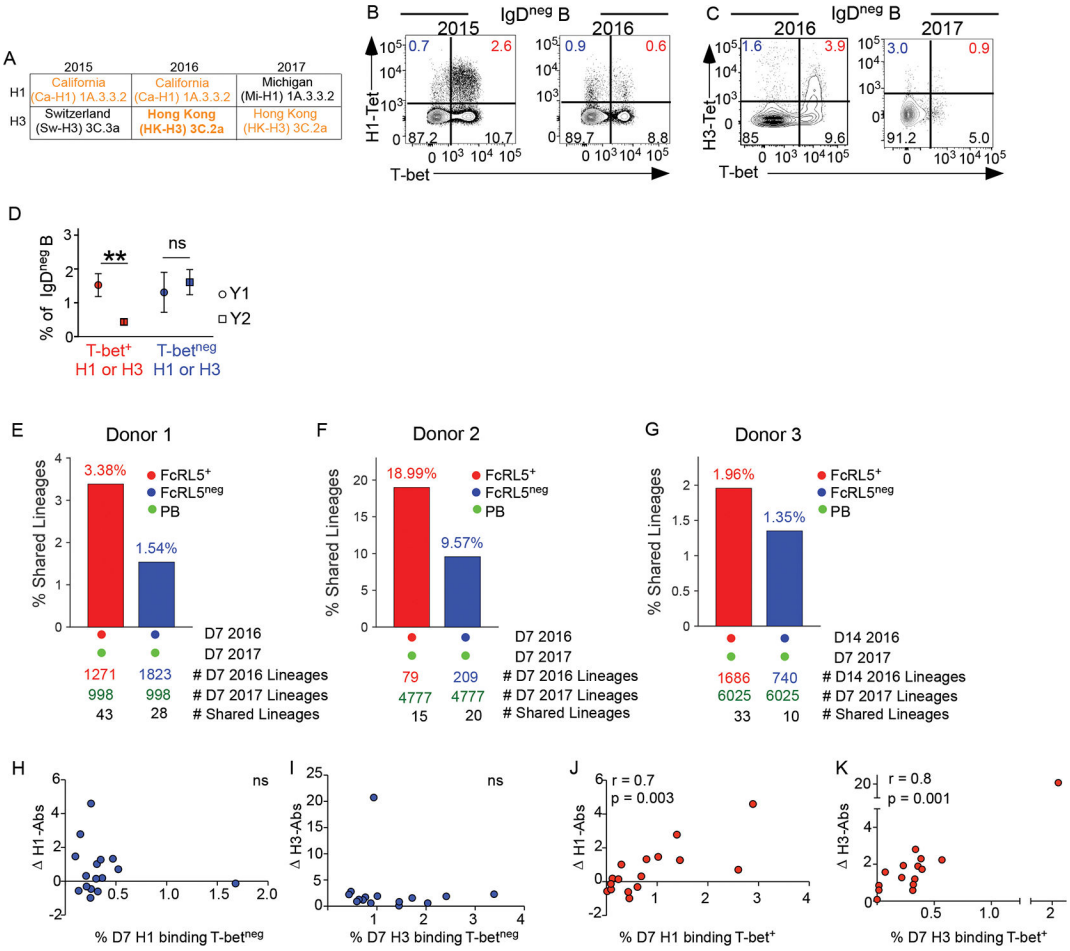

Figure 7. HA-specific IgD^{neg} T-bet^{+} eBmem cells contribute to secondary ASC responses and predict enduring humoral immunity.

(A) Composition of H1 and H3 Ags in 2015–2017 IIV.

(**B-D**) Enumeration of D7 H1- or H3-specific IgD^{neg} T-bet^{+} and T-bet^{neg} B cells in HD sequentially immunized with IIV between 2015 and 2016 (n=6) or between 2016 and 2017 (n=5). FACS analysis showing H1-CA09^{+} Bmem cells over 2 years (2015–2016) from a HD immunized with the same CA09-H1 Ag each year (**B**) or showing HK14-H3 Bmem cells over 2 years (2016–2017) from a HD vaccinated with the same HK14-H3 Ag each year (**C**). Frequencies (**D**), represented as mean with standard error, of the H1-specific or H3-specific T-bet^{+} or T-bet^{neg} B cells for 11 HD vaccinated over 2 years with IIV containing matched H1 or H3 Ags. ** p = 0.002 Wilcoxon matched-pairs signed rank tests.

(**E-G**) V_H BCR repertoire analysis performed on H3-specific IgD^{neg} FcRL5^{+} and FcRL5^{neg} Bmem cells isolated from HDs (n=3) on D7 (**E-F**) or D14 (**G**) post-IIV and PBs isolated from the same donors one year later on D7 following re-vaccination. Data reported as percentage of shared non-singleton lineages between year 1 Bmem cells and year 2 PBs. The number of shared lineages between the PBs and Bmem cell subsets and the number of non-singleton lineages identified by population and timepoint are indicated.

(**H-K**) Correlation analysis of D7 IgD^{neg} HA-specific Bmem cell responses (frequencies in blood, x axis) and vaccine-specific Ab responses (FC in titers between D0 and D120, Y

axis) after IIV in HD (n=19). Comparisons include FC in H1-specific IgG titers vs % D7 H1-specific T-bet^{neg} Bmem cells (**H**); FC in H3-specific IgG titers and % D7 H3-specific T-bet^{neg} Bmem cells (**I**); FC in H1-specific IgG titers and % D7 H1-specific T-bet^{+} Bmem cells (**J**); and FC in H3-specific IgG titers and % D7 H3-specific T-bet^{+} Bmem cells (**K**). Spearman correlation (r) and significance (p) are provided. ns = no significant correlation. See Table S1 for additional correlation analyses.

KEY RESOURCE TABLE.

REAGENT or RESOURCE	SOURCE	IDENTIFIER
Antibodies		
Anti-IgD	BD	Cat# 555778 RRID:AB_396113
Anti-IgD	BD	Cat# 561490 RRID:AB_10679356
Anti-IgD	Biolegend	Cat# 348226 RRID:AB_2561619
Anti-CD19	Biolegend	Cat# 302242 RRID: AB_2561668
Anti-CD19	Biolegend	Cat# 302234 RRID: AB_11142678
Anti-CD19	BD	Cat# 560727 RRID: AB_1727437
Anti-CD27	Biolegend	Cat# 356418 RRID:AB_2562599
Anti-CD3	Biolegend	Cat# 344808 RRID: AB_10640736
Anti-CD3	BD	Cat# 560176 RRID: AB_1645475
Anti-CD4	Biolegend	Cat# 344607 RRID: AB_1953236
Anti-CD4	BD	Cat# 560158 RRID: AB_1645478
Anti-CD14	BD	Cat# 561384 RRID: AB_10611720
Anti-FcRL5	Biolegend	Cat# 340304 RRID: AB_2104588
Anti-CD27	Biolegend	Cat# 356404 RRID: AB_2561788
Anti-CXCR5	Biolegend	Cat# 356904 RRID:AB_2561813
Anti-CCR7	Biolegend	Cat# 353208 RRID:AB_11203894
Anti-CD62L	Biolegend	Cat# 304838 RRID:AB_2562914
Anti-CXCR3	Biolegend	Cat# 353706 RRID:AB_10962912
Anti-CD38	Biolegend	Cat# 303516 RRID: AB_2072782
Anti-T-bet	Biolegend	Cat# 644814 RRID:AB_10901173
Anti-T-bet	Biolegend	Cat# 644812 RRID:AB_2200540
Anti-CD21	Biolegend	Cat# 354908 RRID:AB_2561544
Anti-CD27	Biolegend	Cat# 356418 RRID:AB_2562599
Anti-CD71	BD	Cat# 562995 RRID:AB_2737939

REAGENT or RESOURCE	SOURCE	IDENTIFIER
Anti phosphoS6	Cell Signaling Tech	Cat# 2211 RRID:AB_331679
Anti Rabbit IgG (H+L)	ThermoFisher	Cat# A-21245 RRID:AB_2535813
TotalSeq ™-C0829 anti human FcRL5	Biolegend	Cat# 340309 RRID:AB_2819969
AffiniPure Goat Anti-Human IgG (H+L)	Jackson ImmunoResearch	Cat# 109-005-003 RRID:AB_2337532
Peroxidase Affinipure Goat Anti-Human IgG (H+L)	Jackson ImmunoResearch	Cat# 109-035-088 RRID:AB_2337584
Alkaline Phosphatase AffiniPure Goat Anti-Human IgG (H+L)	Jackson ImmunoResearch	Cat# 109-055-003 RRID:AB_2337599
Bacterial and virus strains		
Biological samples		
PBMCs from flu vaccinated subjects	Alabama Vaccine Research Clinic	N/A
Chemicals, peptides, and recombinant proteins		
H2DCFDA	ThermoFisher	Cat# D399
MitoTracker Green FM	ThermoFisher	Cat# M7514
BODIPY500/510	ThermoFisher	Cat# D3823
Igepal CA-360	Sigma Aldrich	Cat# 18896
Neuraminidase (C. perfringens)	Sigma Aldrich	Cat# N5631
Imidazole	Sigma Aldrich	Cat# 12399
7-ADD (7-aminoactinomycin-D)	ThermoFisher	Cat# A1310
Live/Dead Fixable Near-IR Dead Cell Kit	ThermoFisher	Cat# L10119
Live/Dead Fixable Red Dead Cell Kit	ThermoFisher	Cat# L23102
Formalin solution, 10% neutral buffered	Sigma Aldrich	Cat# HT501128
2-Mercaptoethanol	Thermo Fisher	Cat# BP176-100
Agencourt AMPure XP	Beckman Coulter	Cat# A66514
dNTPs	ThermoFisher	Cat# 18427088
TotalSeq C0952 PE Streptavidin	Biolegend	Cat# 405263
TotalSeq C0953 PE Streptavidin	Biolegend	Cat# 405265
Celltrace Violet	ThermoFisher	Cat# C34557
R848	InvivoGen	Cat# Tlrl-r848

REAGENT or RESOURCE	SOURCE	IDENTIFIER
IL-2	Peprotech	Cat# AF-200-02
IL-21	Peprotech	Cat# AF-200-21
IFN-g	R&D	Cat# 285-IF
Critical commercial assays		
eBioscience Foxp3 Transcription Factor Kit	ThermoFisher	Cat# 00-5523-00
AviTag Kit	Avidity	Cat# BirA-500
RNAeasy Mini Kit	Qiagen	Cat# 74104
Quick RNA Micro Prep Kit	Zymo Research	Cat# R1051
SMART-seq v4 UltraLow Input RNA Kit for Sequencing	Takara	Cat# 634888
NexteraXT DNA library preparation kit	Illumina	Cat# FC-131-1024
EasySep Human B Cell Negative Selection Kit	Stem Cell Technologies	Cat# 17954
Easy Sep Human Pan B Cell Negative Selection Kit	Stem Cell Technologies	Cat# 19554
HiFi Polymerase Mastermix	KAPA Biosystems	Cat# KK2601
Chromium Next GEM Chip G Single Cell Kit 8 rxns	10XGenomics	Cat# 1000120
Chromium NextGEM Single Cell 3’ GEM, Library and Gel Bead Kit v 3.1	10XGenomics	Cat# 1000268
Chromium 3; 5’ Feature Barcode Kit	10XGenomics	Cat# 1000256
Library Construction Kit	10XGenomics	Cat# 1000190
Chemiluminescent Substrate for Alkaline Phosphatase	Moss Inc	ChemiAP-RK100
Deposited data		
Super series of all sequencing data	This paper	Accession# GSE222476
Single Cell sequencing data (RNA-seq and VDJ)	This paper	Accession# GSE222888
RNA-seq	This paper	Accession# GSE163989
ATAC-seq	This paper	Accession# GSE203112
BCR seq	This paper	Accession# GSE222474
Experimental models: Cell lines		
FreeStyle 293F Cells	ThermoFisher	Cat# R79007 RRID:CVCL_D603
Experimental models: Organisms/strains		

REAGENT or RESOURCE	SOURCE	IDENTIFIER
Oligonucleotides		
Vh1a 5'-CAGGTKCAGCTGGTGCAG-3'	Tipton et al. Nat Immunol. 2015.	N/A
Vh1b 5'SAGGTCCAGCTGGTACAG-3'	Tipton et al. Nat Immunol. 2015.	N/A
Vh1c 5' CARATGCAGCTGGTGCAG-3'	Tipton et al. Nat Immunol. 2015.	N/A
Vh2, 5'-CAGGTCACCTTGARGGAG-3'	Tipton et al. Nat Immunol. 2015.	N/A
Vh3, 5'GGTCCCTGAGACTCTCCTGT-3'	Tipton et al. Nat Immunol. 2015.	N/A
Vh4, 5'ACCCTGTCCCTCACCTGC-3'	Tipton et al. Nat Immunol. 2015.	N/A
Vh5, 5'GCAGCTGGTGCAGTCTGGAG-3'	Tipton et al. Nat Immunol. 2015.	N/A
Vh6, 5'CAGGACTGGTGAAGCCCTCG-3'	Tipton et al. Nat Immunol. 2015.	N/A
Vh7, 5'CAGGTGCAGCTGGTGCAA-3'	Tipton et al. Nat Immunol. 2015.	N/A
Cm 5'-CAGGAGACGAGGGGGAAAAGG-3'	Tipton et al. Nat Immunol. 2015.	N/A
Cy 5' CCGATGGGCCCTTGGTGGA-3'	Tipton et al. Nat Immunol. 2015.	N/A
Ca 5'GAAGACCTTGGGGCTGGTCG-3'	Tipton et al. Nat Immunol. 2015.	N/A
F tag, 5' TCGTCGGCAGCGTCAGATGTGTATAAGAGACAG-3'	Tipton et al. Nat Immunol. 2015.	N/A
R tag, 5' GTCTCGTGGGCTCGGGATGTGTATAAGAGACAG-3'	Tipton et al. Nat Immunol. 2015.	N/A
Recombinant DNA		
CA09 Influenza HA (H1)	GeneArt	Protein Sequence Accession: NC_026433.1
SW13 Influenza HA (H3)	GeneArt	Protein Sequence Accession: EPI543739
Michigan 15 Influenza HA (H1)	GeneArt	Protein Sequence Accession: MK622940.1
TX50 Influenza HA (H3)	GeneArt	Protein Sequence Accession: KC892952.1
HK2014 Influenza HA (H3)	GeneArt	Protein Sequence Accession: A0A068IXL
Software and algorithms		
Flowjo v.9.9.3/10.2	FlowJo	N/A
PRISM 8/9	GraphPad	N/A
Seurat v. 3.2.2	Butler et al. Nat. Biotech. 2018.	https://satijalab.org/seurat RRID:SCR_016341
edgeR v3.24.3	Robinson et al. Bioinformatics. 2010.	https://bioconductor.org/packages/release/bioc/html/edgeR.html
SplicingGraphs	Bindreither D et al Bioconductor. 2022.	https://bioconductor.org/packages/SplicingGraphs
Bowtie v1.1.1	Langmead et al. Genome Biology. 2009.	http://bowtie-bio.scourceforg.net/index.shtml RRID:SCR_005476
HOMER	Heinz et al. Mol Cell. 2010.	http://homer.ucsd.edu RRID:SCR_010881
MATLAB	Mathworks	RRID:SCR_001622
IMGT/V-quest v3.5.21	LeFranc et al. Nucleic Acids Research. 2015.	RRID:SCR_010749

REAGENT or RESOURCE	SOURCE	IDENTIFIER
R Project for Statistical Computing	R core team (2018). R: A language and environment for statistical computing. R Foundation for Statistical Computing. Vienna, Austria.	www.R-project.org RRID:SCR_001905
IDEAS Image Data Exploration and Analysis Software	Amnis	RRID:SCR_020142
GSEA	Subramanian, Tamayo et al. PNAS. 102, 15545-15550.	http://www.broadinstitute.org/gsea/ RRID:SCR_003199
IPA	Qiagen	RRID:SCR_008653
Code for single cell RNA-seq analysis	This paper	10.5281/zenodo.7668260
Code for bulk BCR-seq analysis	This paper	10.5281/zenodo.7668260
Code for bulk RNA-seq analysis	This paper	10.5281/zenodo.7672023
Code for bulk ATAC-seq analysis	This paper	10.5281/zenodo.7672023
Other		
2015-2016 Fluzone	Sanofi-Pasteur	National Drug Code: 49281-0396-15
2016-2017 Fluvirin	Sequiris	National Drug Code: 3332-0014-02
2017-2018 Fluzone	Sanofi-Pasteur	National Drug Code: 49281-0417-10
2018-2019 Fluzone	Sanofi-Pasteur	National Drug Code: 49281-0418-10
2020-2021 Fluzone	Sanofi-Pasteur	National Drug Code: 49281-0420-50
Lymphocyte Separation Medium	Sigma Aldrich	Cat# C-44010
Ammonium Chloride Solution	Stem Cell Technologies	Cat# 07800
HisTrap HP Column	GE Healthcare	Cat# GE17-5247-01